Journal of Materials Chemistry C

ROYAL SOCIETY OF CHEMISTRY

REVIEW

View Article Online
View Journal | View Issue

Cite this: J. Mater. Chem. C, 2023, 11, 6800

Research progress of MIL-125 and its modifications in photocatalytic hydrogen evolution

Yijun He, Tianping Lv,* Bin Xiao, Bo Liu, Tong Zhou, Jin Zhang, Yumin Zhang, Genlin Zhang* and Qingju Liu*

MIL-125, a titanium-based metal–organic framework (MOF) material with ultra-high specific surface area, large porosity, tunable structure, modifiable functionality, and multiple active sites, is commonly researched in the field of photocatalytic hydrogen evolution. However, MIL-125 still could not be directly used for practical application in photocatalytic hydrogen evolution because of its limited photoresponse. Therefore, it is necessary to systematically summarize the research on MIL-125 in the field of photocatalytic hydrogen evolution for its further development as well as that of other MOF materials. For MIL-125 photocatalysts, further modifications for promoting the photocatalytic activity of photocatalysts and improving the stability of photocatalysts are needed. Typical modification methods of MIL-125 include engineering functional groups and surface structure, doping metal ions, loading cocatalysts, and structuring composites. In this review, the research progress of MIL-125 in the field of photocatalytic hydrogen evolution is summarized, including its modification methods, photocatalytic hydrogen evolution activities, and micro-mechanisms. In view of the deficiencies and limitations of the current research, future developments of MIL-125 are prospected.

Received 2nd March 2023,
Accepted 2nd May 2023

DOI: 10.1039/d3tc00757j

rsc.li/materials-c

1. Introduction

Over the past few decades, severe environmental pollution and tremendous energy consumption caused by the rapid development of industries have noticeably affected the sustainable development of societies. To solve these problems, it is necessary to develop green and clean energy vigorously.[1] Hydrogen energy is clean, and shows great potential; the related solar-driven water splitting for hydrogen evolution is a very promising research field, in which photocatalysts comprise the core. MOFs are a class of popular microporous materials with high specific surface area, rich and tunable catalytic active sites, and functionalizable organic linkers. They have been widely studied by researchers in many fields.[2–6] Especially, in the field of photocatalysis, many types of MOF materials such as Ru-based MOFs[7] ($[Ru_2(p\text{-}BDC)_2]_n$), Co-based MOFs[8,9] (ZIF-67), Cu-based MOFs[10] (Cu-I-bpy), Ni-based MOFs[11,12] ($[Ni_2(PymS)_4]_n$), Cd-based MOFs[13] (Cd-TBAPy), and Ti-based MOFs[14] (MIL-125) have been studied. Table 1 summarizes the research information of different types of MOFs for photocatalytic hydrogen evolution.

Yunnan Key Laboratory for Micro/Nano Materials & Technology, National Center for International Research on Photoelectric and Energy Materials, School of Materials and Energy, Yunnan University, Kunming 650091, P. R. China. E-mail: qjliu@ynu.edu.cn, lvtp@mail.ynu.edu.cn, 20070019@ynu.edu.cn; Tel: +86 871 65032713

Among them, Ti-based MOF MIL-125 is an attractive material because of its abundant active sites, low reaction potential, high reaction activity, and suitable band gap.[20–22] As shown in Table 1, MIL-125 has an ultra-high specific surface area, as well as the non-toxic and inexpensive properties of Ti-based MOF, which means it has great research potential. In more detail, it is inexpensive and widely available compared with noble-metal-based MOF materials and is also more stable and non-polluting compared with many other free noble-metal-based MOF materials. In 2009, MIL-125 was synthesized for the first time by Dan-Hardi,[23] who discovered its unique optical properties that the new broad and strong absorption peaks were found at 500 nm and 596 nm. Moreover, in 2015, Shen *et al.*[19] first used MIL-125 for photocatalytic water splitting for hydrogen evolution. For a long period of time, MIL-125 had been researched in many other fields such as oxidation and reduction catalytic reactions, energy storage, gas adsorption/separation, and pollutant degradation.[24–32] By searching the Scopus database for the number of published papers related to MIL-125, it can be known that the attractiveness of MIL-125 in academia is increasing year after year (Fig. 1). Attributed to its non-toxic nature, low cost, good biocompatibility, unique optical property, and strong redox ability, MIL-125 exhibited great research value and potential in the field of photocatalysis. Based on the reported research, there are also some reviews related to

Table 1 Summary of different types of MOFs photocatalysts for photocatalytic hydrogen evolution in reported publications

Photocatalysts	Metal center	Specific surface area (m^2 g^{-1})	Bandgap (eV)	Irradiation	Sacrificial agents	Cocatalysts	H_2 evolution rate (mmol h^{-1} g^{-1})	Ref.
$[Ru_2(p\text{-BDC})_2]_n$	Ru	516.5	—	$\lambda > 420$ nm	*N*,*N*′-Dimethyl-4,4′-bipyridinium	—	35	7
g-C_3N_4/ZIF-67/MoS_2	Co	44.2069	—	Solar light	TEOA	—	4.0125	8
Cu-I-bpy	Cu	—	2.00	Solar light	TEA	—	7.09	10
$[Ni_2(PymS)_4]_n$	Ni	—	—	Solar light	TEA	—	25.5	11
Cd-TBAPy	Cd	27	2.15	$\lambda > 420$ nm	TEOA	Pt	0.086	13
Au/Pt-MIL-101	Cr	—	—	$\lambda = 850$ nm	TEOA	Au/Pt	0.1935 (mmol h^{-1} cm^{-2})	15
Ir–Rh/ZrP	Zr	42	—	$\lambda > 420$ nm	TEA	Ir/Rh	0.96	16
AlTCS-1	Al	11	2.54	Solar light	TEOA	—	0.034	17
USTC-8(In)	In	1139	1.79	Solar light	TEA	—	0.3413	18
MIL-125/Pt	Ti	1098.6	—	Solar light	TEOA	Pt	0.1547	19

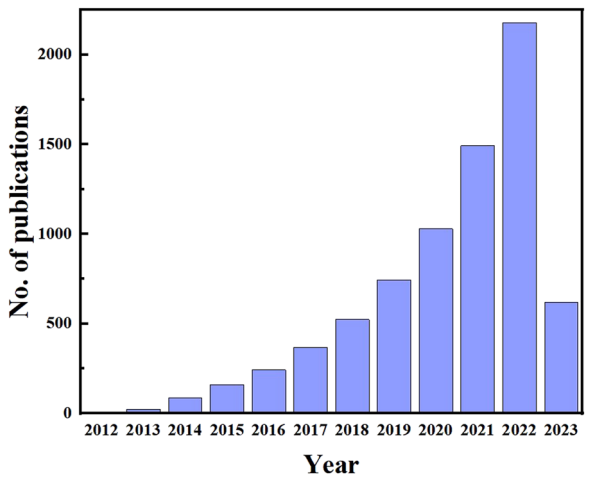

Fig. 1 Number of papers with the subject keyword "MIL-125" in the Scopus database. Statistical time: March 1, 2023.

MIL-125.[33–36] However, this review is of important and distinctive significance for promoting the deeper research of MOF materials and development of photocatalysis.

In the photocatalytic process, light is absorbed by semiconductor materials and electrons are excited for migration from the valence band to the conduction band. Similarly, when MIL-125 is excited by irradiation, electrons transfer from organic ligands to metal active sites *via* the ligand–metal charge transfer pathway, and the unique framework structure makes the electron transfer more adequate and more efficient. However, the limited photoresponse of MIL-125 hindered its practical application. Although the stability of MIL-125 is better than that of other MOF materials due to its high valence cations (Ti^{4+}) and short-size ligands (dicarboxylic acid), it is still less stable than many inorganic materials due to the existence of organic ligands. The structure of MIL-125 may be destroyed by self-decomposition during the photocatalytic reaction. In addition, like many photocatalysts, MIL-125 photocatalysts have limitations such as the shedding of cocatalysts and the photocorrosion of relevant materials. Researchers have conducted many modification methods to enhance the photocatalytic activity and stability. With the modification, promoted carrier separation and migration efficiency will increase the light absorption capacity and finally enhance the photocatalytic activity, and the optimized electron transfer pathway will improve the stability of photocatalysts. Typical modification methods included engineering functional groups and surface structure, doping metal ions, loading cocatalysts, and structuring composites.

This review presents the research progress of MIL-125 in the field of photocatalytic hydrogen evolution and systematically summarizes the modification methods and related mechanisms. Moreover, the development prospects of MIL-125 are proposed according to the shortcomings and limitations of the current research.

2. Structure and properties of MIL-125

MIL-125[23] is a porous crystalline titanium(IV) dicarboxylate material with relatively strong water stability and good photochemical properties, and it can be used as a photocatalyst to provide a stable photoexcited electron platform and broaden the absorption spectrum (Fig. 2). MIL-125 crystallized in a body-centered tetragonal lattice with the *I*4/*mmm* space group (Fig. 2(a)–(c)). The refined lattice parameters are as follows:[37] $a = b = 18.6453(10)$ Å and $c = 18.1444(10)$ Å. Cyclic octamers built from the corner or edge-sharing titanium octahedra and terephthalate anions comprised the framework of MIL-125, which formed a three-dimensional periodic array of mixed tetrahedral and octahedral cages.[38] In addition, the tetrahedral and octahedral cages have inner diameters of 6.1 and 12.5 Å, respectively. The tetrahedral cages could separate molecules by molecular sieving, and the octahedral cages separate molecules based on the differences in packing and the interaction with the pore walls.[39] Based on the special chemical composition and unusual porous structure, MIL-125 has a large specific surface area of 1550 m^2 g^{-1} and a wide band gap energy of 3.6 eV.[40] The high specific surface area of MIL-125 provided abundant active sites, while the broad band gap became its biggest limitation during photocatalysis. Therefore, reducing the band gap of MIL-125 is one of the key points to improving photocatalytic activity, which could improve the carrier transport efficiency. The microscopic composition of MIL-125 can be observed by scanning electron microscopy (SEM), which showed a relatively regular disc-like structure (Fig. 2(d) and (e)).

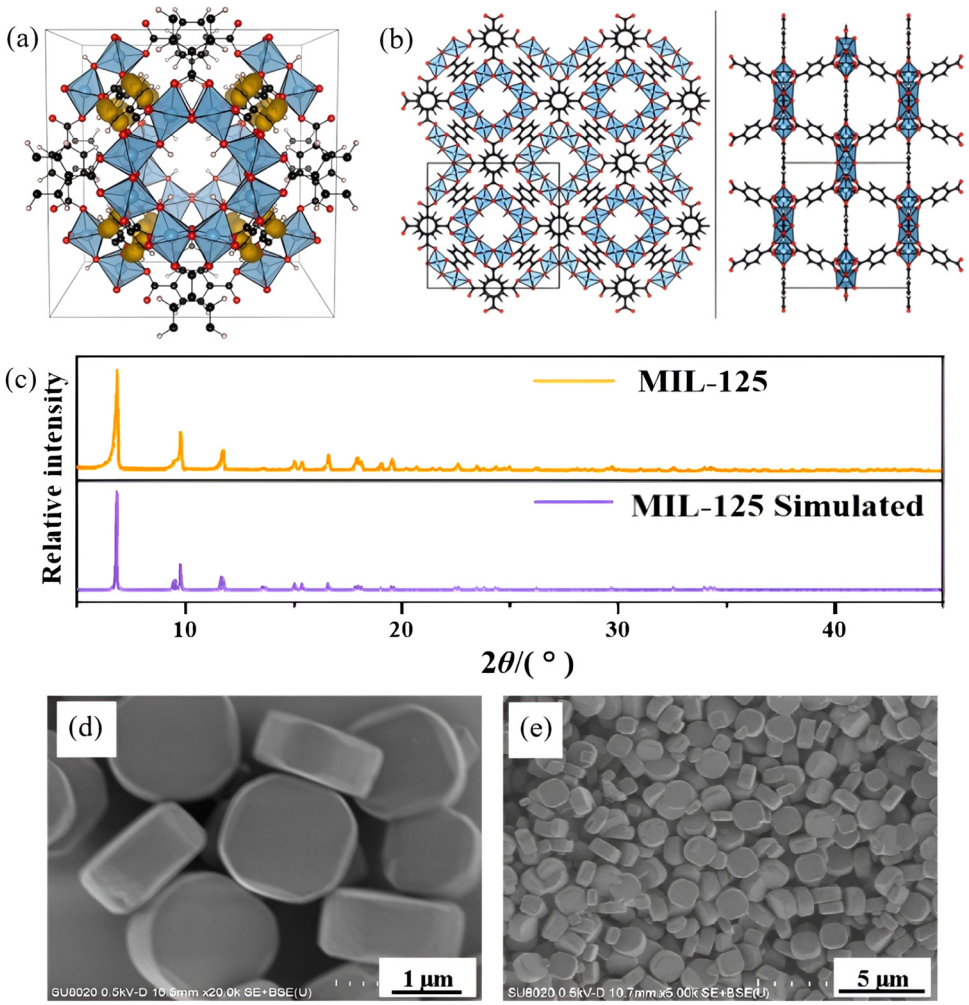

Fig. 2 (a) Schematic diagram of the crystal structure of MIL-125. (b) Crystal orientations of MIL-125: left and right are [001] and [010], respectively. Blue, red, black, and beige represent Ti, O, C, and H, respectively. Reproduced with permission from ref. 38. Copyright 2013, American Chemical Society. (c) XRD patterns of simulated MIL-125 and synthesized MIL-125. (d, e) SEM images of synthesized MIL-125. Reproduced with permission from ref. 41. Copyright 2021, Elsevier.

3. Modification methods of MIL-125

To enhance the hydrogen evolution activity and stability of MIL-125, researchers have made many efforts which included various modification methods. Every modification method has its distinctive mechanism and effects, and they are discussed in categories below.

3.1. Engineering functional groups and surface structure

The engineering of functional groups,[42] which is widely used in the modification of MOF materials, often improves electron migration, changes the energy band structure, and provides unique chemical and optical properties. The engineering of surface structure adjusts the number of facial active sites *via* etching, sensitizing, or defect engineering, which could usually result in enhanced photocatalytic activity.

3.1.1 Engineering of functional groups. The ligands are critical for improving the photocatalytic activity of MIL-125.[43] Many ligands such as amino groups, hydroxyl groups, and methyl groups can be used for MIL-125 modification. Due to its superior chemical properties and optical properties, the amine group, a kind of ring-activating group, is commonly used for MIL-125 modification. In the case of the amino group, MIL-125 was converted into MIL-125-NH_2 *via* replacing the ligands of MIL-125 with mono-aminated bdc-NH_2 linkers, and the band gap of the MOF material was reduced from 3.6 eV to 2.6 eV. When the amino group was incorporated into MIL-125, the 2p orbital electron of N was donated to the aromatic group,[44] resulted in a new red-shifted valence band of MIL-125 and extended the light absorption range to a long wavelength. The amino group could also promote the efficient separation of photogenerated carriers by stabilizing holes.[45] *Via* the solvent-assisted ligand exchange route, the ligand in MIL-125-NH_2 could be partially reversely substituted by 1,4-dicarboxybenzene.[46] The optimized electron transfer efficiency resulted in a higher photocatalytic activity, which was 3.3 times that of pristine MIL-125-NH_2. However, the stability of MIL-125-NH_2 was still not ideal, and the weak oxidation power of the

amino linker[47] made many sacrificial agents such as methanol and triethylamine lose their promoting effects for hydrogen evolution.

It was found that functional group–modified MIL-125 had great potential in dark photocatalysis. Dark photocatalysis[48] usually refers to that reactants storing electrons in the darkness achieve further photocatalytic reactions, which are similar to the natural photocatalysis process. The photocatalytic half-reaction in the dark state is also a kind of dark photocatalysis.[49] In the dark photocatalytic process of MIL-125-X (X = NH_2, Br, NO_2, and none),[50] the electron-donating $-NH_2$ group was beneficial for the generation of Ti^{3+}, while the electron-withdrawing –Br and $-NO_2$ groups were detrimental to Ti^{3+} production (Fig. 3(b)–(g)). Under light, electrons migrated from functional groups to Ti^{4+}, and then under dark conditions, Ti^{3+} released electrons to the surface, which combined with H^+ to produce hydrogen (Fig. 3(a)). The $-NH_2$ group showed more electron density distribution on the cluster and displayed a longer distance between electrons and holes, which resulted in a higher dark photocatalytic activity (Fig. 3(h)–(k)). Christopher *et al.*[38] studied the effects of different groups (–OH, $-CH_3$, –Cl, $-(NH_2)_2$, –Br, and $-CF_3$) on the band gap energy of MIL-125. All the functional groups reduced the band gap energy to different degrees *via* the modification of the valence band, and the diaminated bdc-$(NH_2)_2$ linker, due to its strong electron-donating ability, demonstrated the most significant red-shift with a resulting band gap of 1.28 eV. However, some substituents were not ideal in MIL-125. The crystal with the –Br

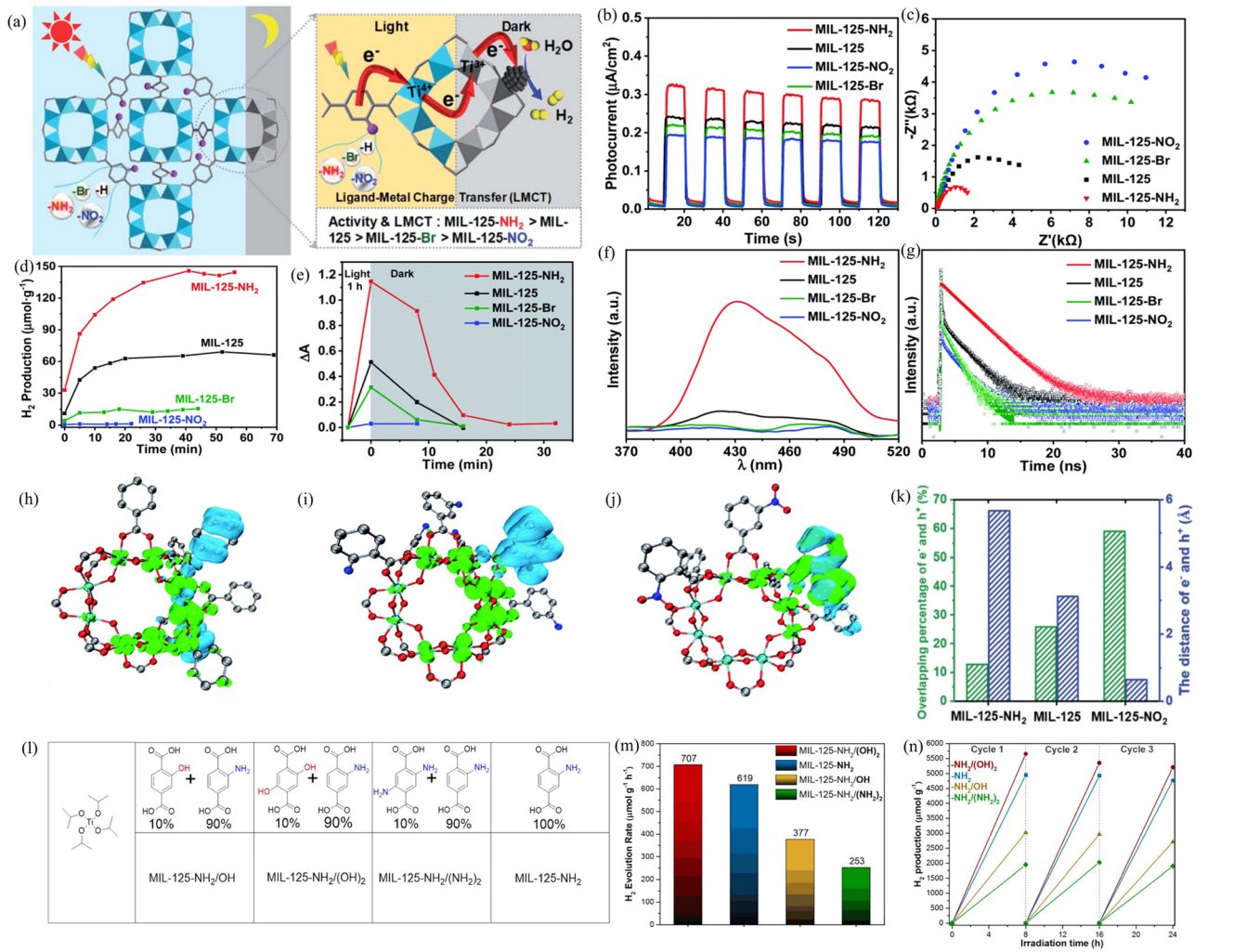

Fig. 3 (a) Illustration of the dark photocatalysis over MIL-125 and MIL-125 with different functional groups. (b) Photocurrent responses, (c) EIS Nyquist plots, and (d) dark photocatalytic hydrogen evolution activity comparison of MIL-125 with different functional groups. (e) Decay profiles of UV-Vis absorption at 530 nm. (f) Photoluminescence (PL) spectra and (g) time-resolved PL spectra for MIL-125 with different functional groups. Electron–hole distribution diagrams of (h) MIL-125, (i) MIL-125-NH_2, and (j) MIL-125-NO_2 in their excited states (red: O; sky blue: Ti; blue: N; gray: C; olive color: electrons; cyan color: holes). (k) Overlapping percentage and distance between electrons and holes in MIL-125 and MIL-125-X (X = NH_2 and NO_2). Reproduced with permission from ref. 50. Copyright 2022, The Royal Society of Chemistry. (l) Tabular representation of MIL-125-NH_2/OH, MIL-125-NH_2/$(OH)_2$, MIL-125-NH_2/$(NH_2)_2$, and MIL-125-NH_2. (m) Photocatalytic H_2 evolution rates and (n) recycling experiments of MIL-125-NH_2/$(OH)_2$ (red), MIL-125-NH_2 (blue), MIL-125-NH_2/OH (yellow), and MIL-125-NH_2/$(NH_2)_2$ (green) with Pt NPs as the cocatalyst. Reproduced with permission from ref. 51. Copyright 2021, American Chemical Society.

group could not be stabilized above eight substitutions per unit cell, and the inclusion of the $-CF_3$ group produced unstable Ti–O bonds. Furthermore, it was reported that[51] MIL-125 with mixed ligands had good photocatalytic activity (Fig. 3(l) and (m)). In MIL-125-NH_2/$(OH)_2$, the chromophoric amino and hydroxyl groups were of good electron-donating ability. The photo-excited electrons migrated from the π-orbital of the organic ligand to the 2p orbital of oxygen and the split 3d orbital of titanium, and then the electrons transferred to the surface of the material to combine with H^+ to evolve hydrogen and the holes would localize to the $-NH_2$ group, and this transfer mechanism promoted effective charge separation. The enhanced p–π conjugation between the lone pairs of O atoms and their aromatic ligands resulted in a red-shifted absorption spectrum. Therefore, the photocatalysts had enhanced hydrogen evolution activity and excellent stability (Fig. 3(m) and (n)).

Protonation[52,53] is another functional group engineering method, which refers to the functionalization of partial functional groups with neutral or negative charges on the surface into positively charged ones, and this is usually applied in the field of adsorption. Notably, it could also promote photocatalytic hydrogen evolution. Luo *et al.*[54] took HCl vapor as the protonation reagent to introduce the $-NH^{3+}Cl^-$ group into MIL-125-NH_2. Because the $-NH^{3+}$ group has positive charges, it could easily interact with negatively charged or partially negatively charged substances such as O or H_2O *via* electrostatic interaction. Therefore, it is conducive to adsorbing H_2O. In protonated MIL-125-NH_2, the $-NH^{3+}$ groups could provide H^+ for hydrogen evolution and the Cl^- site might interact with positively charged species. Hydrogen bonding and electrostatic interaction effectively promoted the separation of photo-induced electron–hole pairs and improved the migration rate of photo-generated carriers. As a result, the hydrogen evolution rate reached 1.69 mmol h^{-1} g^{-1}, which was 20.5 times that of pristine MIL-125-NH_2. However, the pore of the photocatalyst was easily blocked by some organic molecules in the solvent and it resulted in a gradual decrease in the number of accessible active sites over time.

The preparation for the functional group engineering was usually relatively simple because the required product could typically be obtained by one-step synthesis. Such as using the reagent with required functional groups to participate in specific hydrothermal reactions, then the required photocatalyst was synthesized successfully. When selecting for research, it would be necessary to consider the characteristic of each functional group and the interaction between different elements. Table 2 summarizes the effects of different functional groups on the hydrogen evolution activity of MIL-125.

3.1.2 Engineering surface structure. The surface property[55,56] of MIL-125 extremely affects its photocatalytic activity. For photocatalytic materials, a crystal plane with a large proportion of metal clusters usually results in high surface activity.[57]

Crystal facet engineering was used in the modification of MIL-125-NH_2. Guo *et al.*[58] used cetyltrimethylammonium bromide (CTAB) with different concentrations to design and synthesize MIL-125-NH_2 with different exposed facets. Different morphologies were obtained with different etching concentrations (Fig. 4(a)–(e)). Different specific cross-sections correspond to different arrangements of active sites, resulting in the active order of the active surfaces as follows: {110} > {100} > {001} > {111}. The {110} facet contained the biggest amount of metal clusters and performed the most excellent photocatalytic activity, which was three times that of the {111} facet. This indicated that etching can result in better hydrogen evolution activity, and also excellent cycling stability of MIL-125-NH_2 was presented. However, due to the high surface energy,[59] the area of the {110} plane would decrease rapidly during the crystal growth process for minimizing the surface energy. Therefore, the {100} plane became the preferred active plane of MIL-125-NH_2.

Table 2 Summary of the effects of different functional groups on the hydrogen evolution activity of MIL-125 in reported publications

Functional groups	Electronic property	Bandgap (eV)	Characteristic	Ref.
$-NH_2$	Electron-donating	2.6	Favorable	38,50
$-CH_3$	Electron-donating	3.5	Favorable	38
–OH	Electron-donating	2.8	Favorable	38
–Cl	Electron-donating	3.5	Favorable	38
$-CF_3$	Electron-withdrawing	—	Unstable	38
–Br	Electron-donating	3.5	Unstable	38,50
$-(NH_2)_2$	Electron-donating	1.3	Unfavorable	38
$-NO_2$	Electron-withdrawing	3.75	Unfavorable	50
$-NH_2/(OH)_2$	Electron-donating	2.2	Favorable	51
$-NH^{3+}Cl^-$	Electron-withdrawing	2.58	Favorable	54

Defect engineering[60] was also a good modification method for MIL-125. Crystal defects were usually considered a recombination center for excitons and were not conducive to the progress of the photocatalytic reaction.[61,62] However, from another point of view, defect engineering can utilize defects to provide new active sites[63] or to load cocatalysts.[64] Linker defect engineering[65,66] was different from conventional defect engineering. It controlled the coordination environments on metal nodes in MOF materials by removing part of organic linkers in MOF materials while maintaining the structure rigidity or mixed modulators with lower coordination numbers. It can also affect the electron density and electron energy, enhance electronic spin polarization and thus improve the catalytic activity.[67,68] By the linker defect engineering, new additional active sites such as Lewis acid and Brønsted acid sites would be created.[69,70] Yu Horiuchi *et al.*[71] eliminated 18.4% of linkers in MIL-125-NH_2 by the photothermal treatment, which weakened the bonding between linkers and Ti-oxo clusters at the Ti^{3+} sites (Fig. 4(f)). The linker defect sites had become the new additional active sites and the hydrogen evolution activity was the same as that of Pt-loaded MIL-125 under the same condition. However, the research also showed the instability and decomposability of the organic linkers of MIL-125-NH_2. Besides, adjusting the temperature of the water bath can also affect the number of defects of MIL-125-NH_2.[72] Due to the porosity of MIL-125 materials, pore engineering becomes a fascinating modification method for photocatalysis. Naghdi *et al.*[73] took a pyrolysis route to selectively remove one

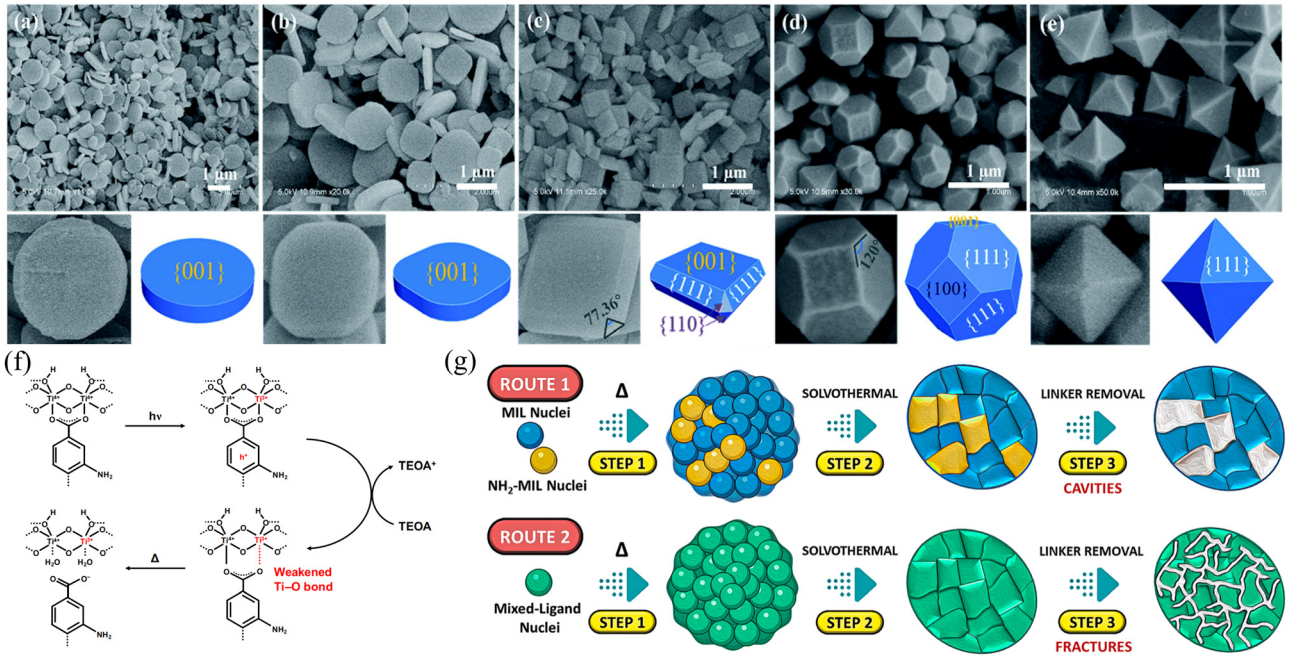

Fig. 4 SEM, enlarged SEM, TEM images, and the 3D geometry models of MIL-125-NH_2 obtained under different concentrations of CTAB: (a) 0, (b) 1 mM, (c) 2 mM, (d) 3 mM, and (e) 4 mM. Reproduced with permission from ref. 58. Copyright 2019, The Royal Society of Chemistry. (f) Proposed mechanism of linker elimination by the photothermal treatment in a water medium containing TEOA. Reproduced with permission from ref. 71. Copyright 2020, Elsevier. (g) Mechanistic model of the MOF formation. Proposed mechanism of the MOF formation *via* a solvothermal process for samples 2–10%NH_2-MIL and 50–80% NH_2-MIL, ranging from the formation of amorphous nuclei to crystals with selective ligand removal. Reproduced with permission from ref. 73. Copyright 2022, Springer Nature.

ligand in mixed-ligand MOFs (MIL-125-NH_2) to introduce additional mesopores. By adjusting the synthesis parameters, cavity-type pores or narrow fracture-type pores can be formed (Fig. 4(g)). The formed new mesopores promoted the diffusion of reactants, and the formation of new active sites enhanced the photocatalytic activity. The fracture-type mesopores with 3D pore connectivity produced a larger specific surface area and were superior to the cavity-type mesopores in enhancing the photocatalytic activity. The enhanced photocatalytic hydrogen evolution rate was 5 times that of the as-prepared MOF, but the stability of the samples was very poor.

Surface structure engineering could improve the photocatalytic activity of MIL-125 by adjusting the number of active sites. The process was relatively simple, but the promoting effect was limited and the photocatalysts were still not stable enough.

3.2. Doping metal ions and loading cocatalysts to MIL-125

Doping metal ions and loading cocatalysts to the MIL-125 surface and interior were effective modification methods to improve the photocatalytic hydrogen evolution activity. Doping metal ions introduced the heterogeneous atoms into the lattice and changed the electron orbital arrangement, and resulted in intermediate energy levels or narrower band gap, and therefore enhanced the photocatalytic activity.[74] For loading cocatalysts, when metal nanoparticles were loaded on the surface of MIL-125 or embedded in its cage, the Schottky barrier would be formed, and the migration and separation of photogenerated carriers would be promoted. Notably, loading cocatalysts into the MIL-125 cage rather than the surface could form a closer contact and more fully utilize the active sites to improve the hydrogen evolution activity.

3.2.1 Doping metal ions. Doping metal ions could optimize the charge transfer pathway of photocatalysts.[75] In the photocatalytic process of MOF materials, the ligand-to-metal charge transfer (LMCT) pathway optimized the electron transport pathway and enhanced the photocatalytic activity by modulating the interaction between ligands and metal clusters.[76] Based on this, Chen *et al.*[77] discovered a new transport mode: ligand-to-linker metal charge transfer (LLMCT) pathway, which formed transient metal centers to facilitate the transfer of electrons from the ligand to metal. The photogenerated electrons participated in the reversible reaction of highly active Cu^{2+}/Cu^{+} mixed centers instead of migrating to the original Ti-oxo-clusters (Fig. 5(a) and (b)). The LLMCT pathway facilitated the delocalization of valence (Fig. 5(c)), boosted the lifetime of photogenerated charges, and increased the carrier density that leads to an increase in photocatalytic activity. Cu-doped MIL-125-NH_2 had high hydrogen evolution activity (Fig. 5(d)) and good cycling stability. Li *et al.*[78] doped Yb into MIL-125-NH_2 to construct Yb^{2+}/Yb^{3+} mixed centers through the analogous mechanism of electron transfer (Fig. 5(e)). The photocatalyst had enhanced the hydrogen evolution activity but was less stable. The research also found that the sacrificial agent triethanolamine was only suitable for weak alkaline conditions. In other words, it was not conducive to hydrogen evolution under acidic, neutral, and strong alkaline conditions. This indicated that

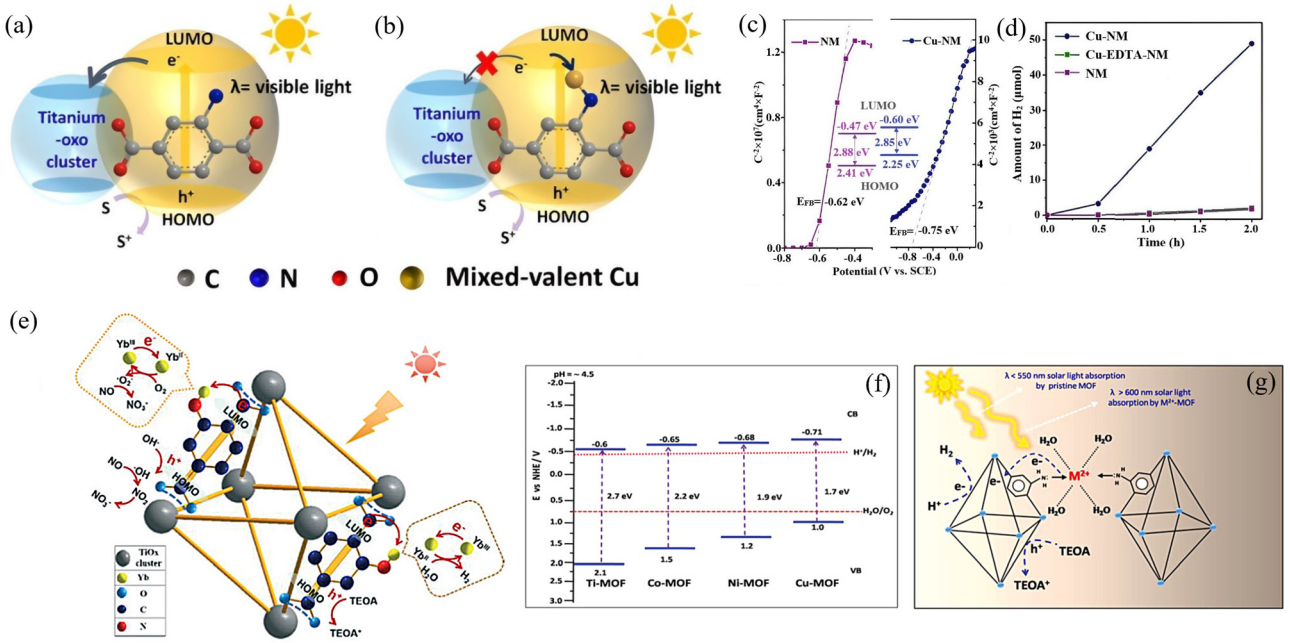

Fig. 5 Schematic diagram of the electron transfer pathways from an organic linker to (a) a titanium-oxo cluster in MIL-125-NH_2 and (b) a mixed-valence Cu center. (c) Mott–Schottky plots of NM and Cu-NM. (d) Performance of Cu-NM *vs.* Cu-EDTA-NM in photocatalytic H_2 evolution. Reproduced with permission from ref. 77. Copyright 2020, Wiley-VCH Verlag GmbH & Co. KGaA, Weinheim. (e) Proposed mechanism for the removal of NO and efficient hydrogen evolution of Yb-NM-X under light irradiation. Reproduced with permission from ref. 78. Copyright 2021, The Royal Society of Chemistry. (f) Band energy alignments with respect to M^{2+} ion coordination. (g) Possible mechanism for photocatalytic H_2 production. Reproduced with permission from ref. 80. Copyright 2019, WILEY-VCH Verlag GmbH & Co. KGaA, Weinheim.

pH had a significant effect on photocatalytic activity. Zhang *et al.*[79] installed high-valent W^{6+} ions onto the Ti-oxo clusters of MIL-125. The formation of the W–O–Ti bond optimized the charge transport path and the photocatalytic hydrogen evolution rate had increased by 4 times. Ti-oxo clusters had the electron-withdrawing ability and the more positive valence state of W^{6+} sites attracted holes from the titanium-oxo cluster, therefore the charge separation and charge migration were promoted effectively. Neppolian *et al.*[80] found the strong coordination of transition metal ions with MIL-125-NH_2 and other MOFs significantly improved the optical absorption by d–d transitions and the multi-metal sites facilitated the fast separation of charges, which promoted the photocatalytic activity (Fig. 5(f) and (g)).

Doping metal ions into MOF materials could improve the electron transfer pathway, but it cannot improve the stability, and the enhancement of photocatalytic activity was usually not significant.

3.2.2 Loading cocatalysts on the surface of MIL-125. MIL-125 has a large specific surface area to expose numerous active sites.[81] Loading metal cocatalysts could construct new active sites on the surface of MIL-125 for photocatalytic hydrogen evolution, such as the deposition of noble metals: Pt[82] and Pd.[83] Due to the higher work function of metal cocatalysts, photogenerated electrons prefer to transfer to the metal atoms and this is beneficial for the effective separation of charges. An appropriate amount of cocatalysts could effectively restrain the recombination of carriers and enhance hydrogen evolution activity. Excessive cocatalysts usually restrain the light absorption of the photocatalysts. The synthesis process of loading on the surface would result in the partial loading of cocatalysts in the cage, which is unavoidable.

The excellent synergy between Ni_2P and MIL-125-NH_2[84] was found when compared with other transition metal phosphide and oxide cocatalysts (CoP, Co_3O_4, Fe_2O_3, and CuO). Falletta *et al.*[85] researched the electron transfer mechanism of MIL-125-NH_2/NiO/H_2O and MIL-125-NH_2/Ni_2P/H_2O. The photogenerated electrons transferred from MIL-125-NH_2 to Ni_2P and NiO and then reaction with H^+ for hydrogen evolution (Fig. 6(a)). Using the designed potential calculation principle, the difference between them was found by the calculation of electron affinities between NiO and Ni_2P. Subsequently, they took the vacuum energy level as the average electrostatic potential of the pore center and found that the band gap of MIL-125-NH_2 was below 6.8 eV under the vacuum level (Fig. 6(b) and (c)). The band gap arrangement of MIL-125-NH_2/NiO/H_2O and MIL-125-NH_2/Ni_2P/H_2O was obtained *via* a series of calculations (Fig. 6(d)). Fluorescence emission resulted from the photogenerated carriers of the MOF quenched when Ni_2P was loaded into MIL-125-NH_2, and this indicated that the carrier recombination was suppressed. However, in the case of NiO, it only partially affected the light emission and formed a larger gap between the conduction band energy level and hydrogen reduction energy level and resulted in photo-induced quenching. According to the Marcus theory,[86] the energy difference between the donors and acceptors represents the driving force

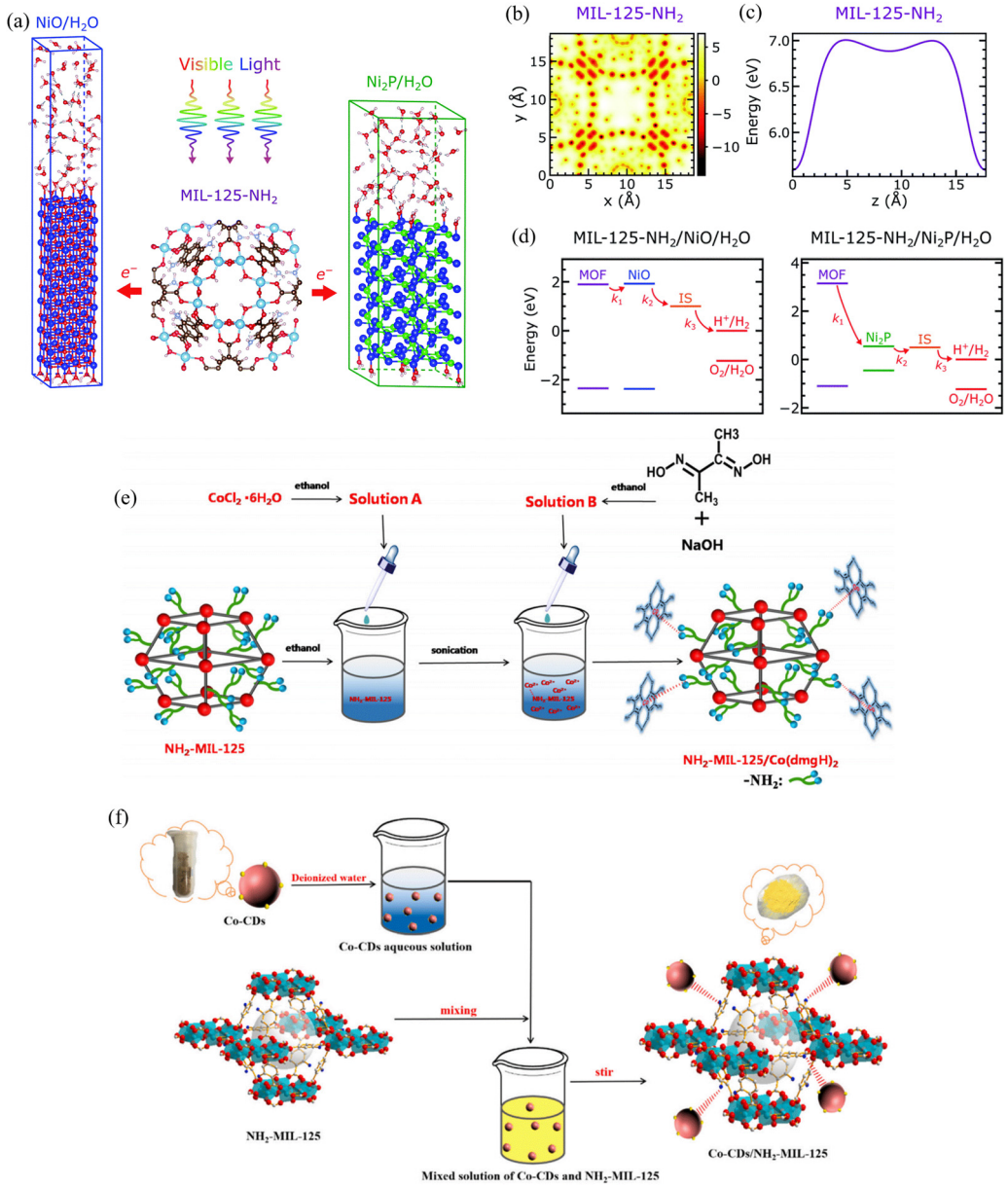

Fig. 6 (a) Schematic diagram of the composite MIL-125-NH_2/NiO/H_2O and MIL-125-NH_2/Ni_2P/H_2O photocatalytic interfaces. (b) Electrostatic potential in MIL-125-NH_2 averaged over the direction *z*. (c) Electrostatic potential in MIL-125-NH_2 along the line parallel to *z* and intersecting the plane *xy* at the center of the pore. (d) Alignment of the band edges at the composite MIL-125-NH_2/NiO/H_2O and MIL-125-NH_2/Ni_2P/H_2O interfaces. Reproduced with permission from ref. 85. Copyright 2020, The Royal Society of Chemistry. (e) Synthesis of NH_2-MIL-125/Co(dmgH)$_2$. Reproduced with permission from ref. 87. Copyright 2020, Elsevier. (f) Synthetic route of Co-CDs/NM. Reproduced with permission from ref. 88. Copyright 2022, Elsevier.

for electron transfer, so it indicated that NiO had a greater photocatalytic activity in MIL-125-NH_2.

The potential for the photocatalytic proton reduction of Co(dmgH)$_2$ was found.[89] Luo *et al.*[87] used simple solution mixing preparation to synthesize NH_2-MIL-125/Co(dmgH)$_2$ (Fig. 6(e)). Flower-like Co(dmgH)$_2$ particles loaded on the surface of MIL-125-NH_2 promoted the separation of the carriers. In the photocatalytic reaction, the Co^I substance of Co(dmgH)$_2$ accepted an electron and transferred to Co^{III}-hydride, and then another proton source protonated the Co^{III}-hydride to produce H_2 during heterolytic decomposition. The photocatalyst performed a high hydrogen evolution activity under visible light. Co_3O_4 was a good cocatalyst for MIL-125-NH_2. However, when it loaded on the defective MIL-125-NH_2 rather than pristine MIL-125-NH_2, the photocatalytic activity was lower due to the inefficient electron transfer.[90]

Non-metallic cocatalysts were also used to enhance the photocatalytic activity. Carbon nanodots[91,92] were zero-dimensional nanomaterials with unique up-conversion effect and excellent electron transfer ability. Their optical property depended on their size, edge shape, surface ligands, and defects.[93,94] He *et al.*[88] loaded Co^{2+}-passivated carbon nanodots on the surface

of MIL-125-NH_2 *via* simple solution mixing preparation (Fig. 6(f)), and the carbon nanodots with a particle size of mainly about 1.6–1.8 nm were evenly distributed on the surface of MIL-125-NH_2. Due to the up-conversion effect, the long-wavelength light absorbed by carbon nanodots was converted into short-wavelength light and emitted, resulting in improved light absorption. The hydroxyl groups and carboxyl groups on the surface of the carbon nanodots interacted with the amino groups of MIL-125-NH_2 and promoted the transfer of electrons. Due to the charge repulsion, Co^{2+} promoted the carbonization of carbon nanodots and also optimized the electron transfer pathway. The hydrogen evolution activity of the photocatalyst increased by 6.86 times that of the original MIL-125-NH_2.

Due to the special porous framework structure of MIL-125, cocatalysts with a large particle size would be loaded on the surface of MIL-125 rather than the interior. Therefore, it is necessary to consider the appropriate amount of cocatalysts and choose more reasonable preparation routes to avoid restraining light absorption and control the particle size of cocatalysts, respectively.

3.2.3 Packaging cocatalysts in the cages of MIL-125. The encapsulation of cocatalysts into the cages of MIL-125 can fully utilize the long-range ordered porous structure of the MOF material and allow for more active sites to participate in photocatalytic reactions. MIL-125 has a tetrahedral cage and an octahedral cage with internal diameters of 6.1 and 12.5 Å, respectively. Whether the particle size of cocatalysts is smaller than that of the pore size of MIL-125 is the key to designing encapsulation. Single-atom cocatalysts[95] can be well dispersed into the pores of MIL-125 due to the atomic-levelled particle size. The cocatalysts which encapsulated in the cages can usually be synthesized by the ionic substances reduced into the 0-valent substances.

When nanostructured metal cocatalysts (such as Au, Ag) contacted with the semiconductors or semiconductor-like materials, the plasmonic hot electrons would be injected into the lowest unoccupied molecular orbital (LUMO) and the widened conduction band resulted in the reduced band gap energy. Xiao *et al.*[96] prepared a Pt@MIL-125/Au catalyst, which had two types of metal–MOF interfaces. Surface plasmonic resonance excitation of Au nanorods promoted the separation of the photogenerated carriers and extended the light absorption to the visible light and resulted in a new absorption band at 700 nm. In addition, Pt with high work function[97] dispersed in MIL-125 and formed a Pt-MIL-125 Schottky junction. As the Pt nanoparticles were pre-introduced into the reactants for the preparation of MIL-125, the size of Pt nanoparticles remained about 3 nm. The hydrogen evolution rate of Pt@MIL-125/Au reached 1.743 mmol h^{-1} g^{-1}, which was 10 times higher than that of Pt/MIL-125/Au and the photocatalyst had high stability. Huang *et al.*[98] dispersed Pt clusters into MIL-125-NH-CH_2OH *via* the *in situ* auto-reduction route. When amino groups reacted with formaldehyde and resulted in the generation of reducing groups, Pt^{2+} was *in situ* reduced to ultra-small Pt clusters; thus, the content of Pt was raised. The reduction route which introduced Pt nanoclusters into the cage of MIL-125 highly enhanced the photocatalytic activity. Different synthesis routes would greatly affect photocatalytic activity. Pd nanoparticles prepared *via* the photo-assisted deposition route were smaller and more dispersed than the conventional ion exchange approach.[99] It formed more active sites to participate in photocatalytic hydrogen evolution.

Some distinctive synthesis routes to introduce cocatalysts into the MIL-125 cage were reported. Nasalevich *et al.*[100] assembled cobaloxime-derived active sites in the organic cavity by a unique Ship-in-a-Bottle strategy to introduce Co into MIL-125-NH_2. The synthesis route is as follows: first, the flexible organic component L^{H2}: $(DOH)_2pn$ was mixed into the solution of MIL-125-NH_2, at which time L^{H2} entered the cage of MIL-125-NH_2. Then, $CoBr_2{\cdot}6H_2O$ was added to the solution under air condition and resulted in the final Co@MOF materials. The redox potential of the cobalt species was higher than that of MIL-125-NH_2 and thus the photogenerated electrons preferred to transfer to the Co active sites and resulted in the promoted separation of carriers.[101] The photocatalytic activity was increased by 20 times compared with pristine MIL-125-NH_2 and the photocatalyst had excellent stability. Furthermore, Li *et al.*[102] diffused flexible TPA ligands into the cages of MIL-125-NH_2, and then introduced Co^{2+} cations to form rigid Co^{2+} complexes (Fig. 7(a)). MIL-125-NH_2 provided a heterogeneous platform to disperse Co^{2+} complexes, and the reduction potential of Co^{2+}/Co^{+} was between the conduction band potential of MOFs and hydrogen evolution potential and thus formed an effective charge transfer pathway for photocatalytic hydrogen evolution (Fig. 7(b)). Two electron transfer mechanisms were proposed, and it was found that only the second route occurred or at least was dominant in it (Fig. 7(c) and (d)). The Co substances significantly enhanced the hydrogen evolution activity and the hydrogen evolution rate reached 553 μmol h^{-1} g^{-1}, which was 14.9 times higher than that of the physical mixture under the same Co loading. In addition, the photocatalyst also had superior cycling stability. It revealed the advantages of encapsulation in promoting electron transfer and enhancing photocatalytic activity.

He *et al.*[103] used an *in situ* calcination route to embed carbon nanodots (CDs) into the cages of MIL-125-NH_2. The prepared MIL-125-NH_2 was immersed in the glucose solution and stirred at room temperature, and then the samples were washed several times with EtOH/H_2O (9 : 1) to remove surface-adsorbed glucose. Subsequently, the glucose-loaded MIL-125-NH_2 was calcined under nitrogen flow, and finally, the CDs@MIL-125-NH_2 was obtained. Due to the up-conversion effect of the carbon nanodots, the near infrared-visible light was converted into the ultraviolet-visible light and resulted in enhanced light absorption. The hydroxyl groups and carboxyl groups on the surface of the carbon dots interacted with the amino groups of MIL-125-NH_2 and promoted the efficient electron transfer. The hydrogen evolution rate was increased to 5.3 times that of the original MIL-125-NH_2. However, the stability of the photocatalyst was poor.

Metal single-atom photocatalysts are attractive in the field of photocatalysis due to their extraordinary photocatalytic activities. However, the high surface energy of materials

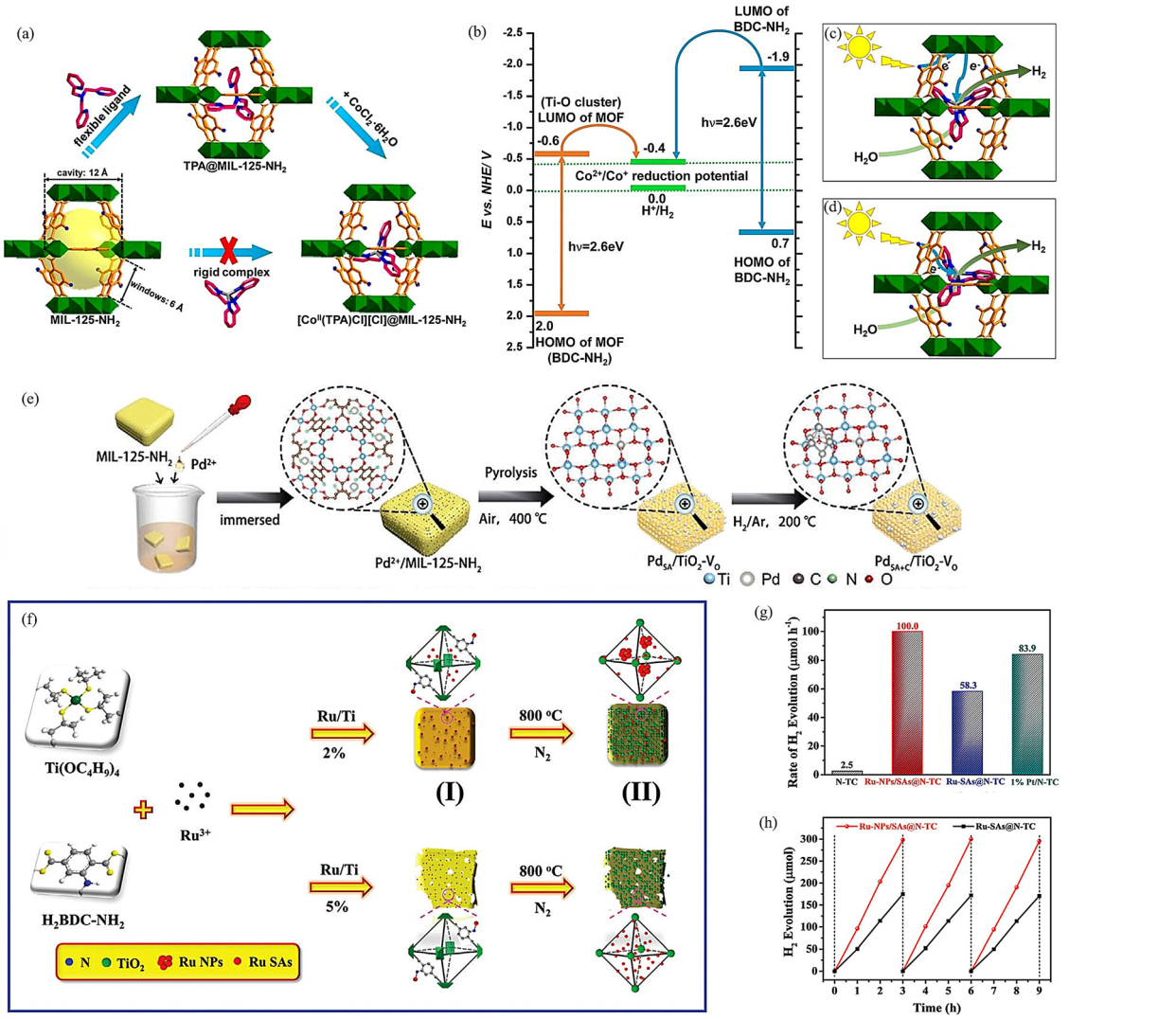

Fig. 7 (a) Schematic illustration of the "Ship-in-a-Bottle" strategy. (b) Schematic diagram of redox potentials of MIL-125-NH_2, BDC-NH_2, Co^{2+} Complex, and H^+/H_2. Proposed electron transfer route (c) between MIL-125-NH_2 and the Co^{2+} complex; and (d) between BDC-NH_2 and the Co^{2+} Complex. Reproduced with permission from ref. 102. Copyright 2016, American Chemical Society. (e) Schematic diagram of the preparation of Pd_{SA}/TiO_2-V_O and Pd_{SA+C}/TiO_2-V_O photocatalysts. Reproduced with permission from ref. 107. Copyright 2020, Wiley-VCH GmbH. (f) Schematic illustration of the preparation of Ru-NPs/SAs@N-TC and Ru-SAs@N-TC samples. (g) H_2 evolution rates of different samples under simulated solar light. (h) Photostability of H_2 evolution of Ru-NPs/SAs@N-TC and Ru-SAs@N-TC. Reproduced with permission from ref. 109. Copyright 2020, WILEY-VCH Verlag GmbH & Co. KGaA, Weinheim.

restrains the anchor in the substrate. Due to the unsaturated coordination of atoms at the defects, the surface defects could easily anchor single atoms.[104] Therefore, defect engineering was a suitable synthesis route for loading single-atom cocatalysts. Cu single atoms presented very superior photocatalytic activity.[105] Cu single atoms with unsaturated coordination loaded in TiO_2 with oxygen vacancies,[106] and the adsorption of water molecules was facilitated and the hydrogen evolution activity of the photocatalyst was significantly improved. Zhang *et al.*[95] introduced Cu into MIL-125 and then derived it into TiO_2 with anchored Cu single atoms, and it significantly enhanced the hydrogen evolution activity and the photocatalyst had excellent stability. It can be observed that the Cu single atoms were uniformly dispersed in the cage of TiO_2. Wang *et al.*[107] used a similar route to obtain TiO_2 with loaded Pd single atoms and it had excellent hydrogen evolution activity (Fig. 7(e)). Moreover, Lv *et al.*[108] further studied the coordination between the Pd sub-nanoclusters and the Pd single atoms on the substrate of TiO_2 and found that the Pd sub-nanoclusters can effectively promote the electron transfer of the Pd single atoms. It further improved the hydrogen evolution activity and the photocatalyst had excellent stability. Yan *et al.*[109] took MIL-125-NH_2 with doped Ru^{3+} as a precursor to prepare TiO_2 with anchored Ru single atoms (Fig. 7(f)). By adjusting the initial addition amount of Ru^{3+}, the dispersion state of Ru species was regulated. The optimal hydrogen evolution rate was 40 times that of the pristine N-doped TiO_2/C and the stability of the photocatalyst was pleasant (Fig. 7(g) and (h)). It can be seen that single-atom

modifications show great potential in MIL-125-based photocatalysts for photocatalytic hydrogen evolution.

Compared with the loading on the surface of MIL-125, the modification methods to load cocatalysts into the cages of MIL-125 can make better use of the porous framework structure because the numerous active sites in the pores could be utilized for enhancing hydrogen evolution. However, it is highly demanding, and usually, a relatively complicated synthesis is needed, which means it has limitation in the synthesis of some large-sized materials. In comparison, the advantages of loading on the surface of MIL-125 are the simplicity of the preparation process and the variety of alternative synthesis and available materials. This is the reason for the extensive use of this method. However, cocatalysts at the surface are more likely to fall off during the reaction process, resulting in poor stability. Moreover, only the active sites on the surface are utilized while the internal active sites are wasted, which resulted in a lower photocatalytic activity.

The current research studies related to doping and loading in MIL-125 for photocatalytic hydrogen evolution are summarized in Table 3.

3.3. MIL-125 composite photocatalysts

The use of appropriate substances to construct heterojunctions could promote the separation and transfer of photogenerated carriers and improve the photocatalytic activity. Many materials such as metal oxides,[116,117] metal sulfides,[118] carbonitrides,[119] alloys,[120] and organics[121] have been developed for MIL-125 composite photocatalysts.

3.3.1 Composite materials with metal sulfides. CdS was a common photocatalyst material,[122,123] but its photocatalytic activity was limited by the strong oxidation and the high agglomeration tendency. The combination with other wide bandgap semiconductors or semiconductor-like materials could restrain these problems.[118] Due to their suitable energy band structures, CdS and MIL-125 can form heterojunctions for enhancing photocatalytic hydrogen evolution. Tai *et al.*[82] used the γ-ray irradiation synthesis route[124] to uniformly disperse Pt and CdS nanoparticles into the interior and surface of MIL-125, respectively (Fig. 8(a)). This route avoided the contamination by chemical-reducing agents and active agents. The photocatalytic hydrogen evolution was facilitated by the optimized carrier transport pathway, but the stability of the photocatalyst was not ideal. Zhang *et al.*[125] prepared a *Z*-scheme CdS/MIL-125-NH_2 heterojunction photocatalyst with CdS nanoparticles embedded on the surface of MIL-125-NH_2. When the photocatalyst was excited by light, the photogenerated electrons transferred from the valence band of MIL-125-NH_2 to its conduction band and then transferred to the valence band of CdS. Meanwhile, the CdS was also excited by light and the photogenerated electrons transferred from the valence band of it to its conduction band, and finally, the photogenerated electrons transferred to the hydrogen reduction level to combine with H^+ to evolve H_2. It was an example of the electron transfer pathway of the *Z*-scheme heterojunction photocatalyst. The *Z*-scheme heterojunction had the advantages of promoting the efficient separation of carriers and retaining the stronger polarity of potential, which enhanced the redox ability.[126] The improved hydrogen evolution rate of the photocatalyst under visible light was 3.5 times higher than that of pristine CdS. However, the stability of the photocatalyst was not ideal. A *Z*-scheme MIL-125-NH_2/Ti_3C_2 QDs/$ZnIn_2S_4$ photocatalyst had a similar mechanism.[127] In the photocatalytic system, Ti_3C_2 QDs acted as electron transfer mediators, which promoted the electron transfer (Fig. 8(b)).

Li *et al.*[128] constructed an *S*-scheme heterojunction photocatalyst of MIL-125-NH_2/$Zn_{0.5}Cd_{0.5}S$ mediated by C_{60} *via* a series of synthesis (Fig. 8(c)). C_{60} was a good intermediate for promoting the transfer of photoelectrons, because the conical arrangement of carbon atoms and conjugated large π bonds facilitated the transfer and separation of photogenerated carriers.[129] In the *S*-scheme heterojunction, carriers with strong redox ability participated in the hydrogen evolution reaction, and carriers with weak redox ability were consumed. The distinctive

Table 3 Summary of doping and loading in MIL-125 photocatalysts for photocatalytic hydrogen evolution in reported publications

Photocatalysts	Specific surface area ($m^2\ g^{-1}$)	Bandgap (eV)	Irradiation	Sacrificial agents	Cocatalysts	H_2 evolution rate (mmol $h^{-1}\ g^{-1}$)	Ref.
Pt/MIL-125-NH_2/$(OH)_2$	1147	2.2	Visible	TEOA	Pt	0.707	51
Yb-NH_2-MIL-125	—	2.37	Visible	TEOA	Pt	1.884	78
W-MIL-125	921.6	2.75	UV-vis	TEOA	Pt	1.11	79
MIL-125-CoPi-Pt	511.014	—	UV-vis	MeOH	CoPi/Pt	0.063	97
Pt/MIL-125-NH-CH_2	—	2.76	Visible	Formaldehyde/ethanol	Pt	4.496	98
Ni_2P/MIL-125-NH_2	27.8	—	Visible	TEOA	Ni_2P	0.894	110
MIL-125-NH_2/Ni_2P	—	—	Visible	—	Ni_2P	1.23	85
Pt@MIL-125/Au	986	3.72	UV-vis	MeCN/TEOA	Pt/Au	1.743	96
Co@NH_2-MIL-125	—	2.59	Visible	TEA	Co	0.62	100
Co(II)@MIL-125-NH_2	855	2.6	Visible	TEOA	Co(II)	0.553	102
CDs@NH_2-MIL-125	1312.13	2.42	Visible	TEOA	Pt	5.82	103
1T-MoS_2/MIL-125-NH_2	990	—	Visible	TEA	1T-MoS_2	1.454	111
CoP/MIL-125-NH_2	484	—	Visible	TEOA	CoP	6.19	112
Pt-RuO_x-MIL-125-NH_2	1200	2.45	UV-vis	MeOH	Pt/RuO_x	9.083	113
NH_2-MIL-125@Ni $(OH)_2$	—	2.25	Visible	TEOA	Ni $(OH)_2$	0.126	114
Au@NH_2-MIL-125(Cu/Ti)	1094.37	2.43	Visible	TEOA	Pt/Au	1.039	115
CdS/Pt/MIL-125	194.9	2.34	Visible	Na_2S/Na_2SO_3	CdS/Pt	6.78	82
Pd-MIL-125-NH_2	948	—	—	HCOOH	—	0.320	83

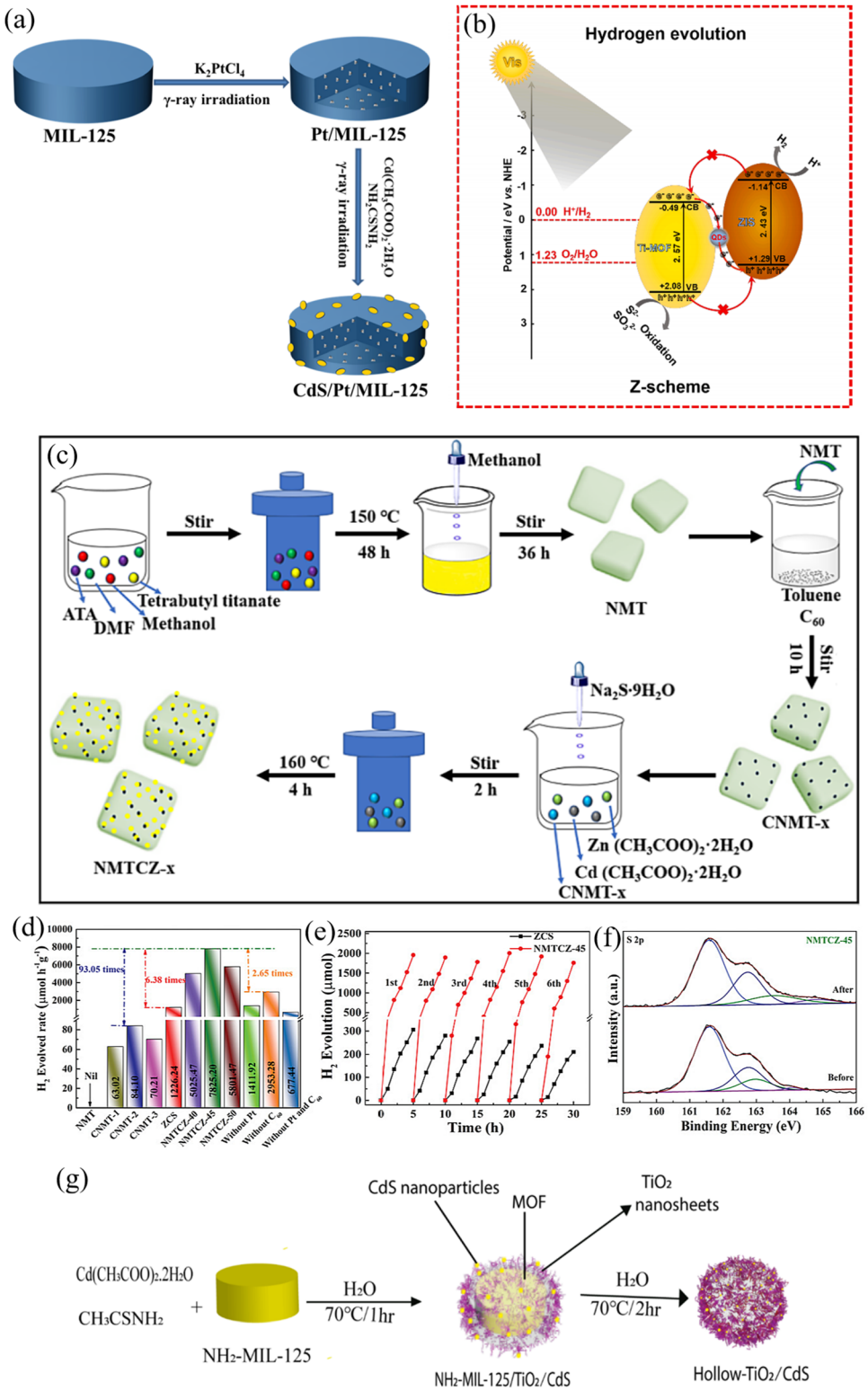

Fig. 8 (a) Synthesis process for CdS/Pt/MIL-125 composites using γ-ray irradiation. Reproduced with permission from ref. 82. Copyright 2020, American Chemical Society. (b) Possible photocatalytic mechanisms for hydrogen evolution on the *Z*-scheme Ti-MOF/QDs/ZIS composite photocatalyst under visible light irradiation. Reproduced with permission from ref. 127. Copyright 2022, Elsevier. (c) Preparation process of the NMTCZ-x *S*-scheme heterojunction. (d) PHE activity of samples under visible-light illumination. (e) Cycle experiments. (f) S 2p XPS of NMTCZ-45 before and after six cycles. Reproduced with permission from ref. 128. Copyright 2021, Wiley-VCH GmbH. (g) Synthetic procedure of the NH_2-MIL-125/TiO_2/CdS yolk–shell and hollow-TiO_2/CdS heterostructures. Reproduced with permission from ref. 130. Copyright 2018, American Chemical Society.

charge transfer pathway also significantly improved the stability of the photocatalysts by restraining the photocorrosion of sulfides. Therefore, the photocatalyst had enhanced the hydrogen evolution activity, which was 93.05 times and 6.38 times higher than that of C_{60}/MIL-125-NH_2 and $Zn_{0.5}Cd_{0.5}S$, respectively (Fig. 8(d)), and had excellent stability compared to pristine $Zn_{0.5}Cd_{0.5}S$ (Fig. 8(e) and (f)).

Ternary heterojunction photocatalysts had potential to further improve the photocatalytic activity. Bibi *et al.*[130] prepared yolk–shell type MIL-125-NH_2/TiO_2/CdS and hollow-TiO_2/CdS heterostructure photocatalysts *via* a post solvothermal route (Fig. 8(g)). TiO_2 nanosheets were connected with the amino groups of MIL-125-NH_2 *via* Ti–O–N bonds, resulted in the heterojunction between TiO_2 and MIL-125-NH_2, and optimized the electron transfer pathway. The incorporation of CdS nanoparticles further improved the separation efficiency of carriers and enhanced the absorption of visible light. The heterostructure had remarkable photocatalytic activity which was 18 times greater than that of pristine CdS, and the photocatalyst had good stability. Hierarchical tandem heterojunctions,[131] which usually had three or more components, were more favorable structures for improving the photocatalytic activity. When the photocatalyst was illuminated, photogenerated electrons were transferred from both sides to the surface of the intermediate component, where the hydrogen evolution occurred. Zhang *et al.*[132] constructed a mesoporous MIL-125-NH_2@$ZnIn_2S_4$/CdS hierarchical tandem heterojunction photocatalyst *via* a two-step solvothermal and one-step hydrothermal route. The enrichment of interfacial electrons led to higher separation and transfer efficiency of carriers, and the double-electron transfer mechanism of CdS and MIL-125-NH_2 inhibited the photocorrosion of CdS, which made a contribution to stability. The core–shell structure also improved the stability of the photocatalyst by weakening the aqueous corrosion of titanium oxide clusters. The reduced electron transfer distance and the increase in exposed active sites were positive for enhancing photocatalytic hydrogen evolution. Therefore, the hydrogen evolution rate under visible light was 2.367 mmol h^{-1} g^{-1} and the band gap energy of the photocatalyst was only 1.84 eV. The hydrogen evolution rate remained almost constant after 25 hours of working, which shows the excellent stability of the photocatalyst. However, the photocatalyst had a relatively complicated preparation procedure, and like most powder photocatalysts, it was difficult to recycle. Besides, cadmium ions are harmful to the environment, and hence, it is necessary to develop environmentally friendly photocatalysts to replace harmful photocatalysts.

Current metal sulfide photocatalysts usually had the suitable band gaps and superior photocatalytic activities, but they also had the disadvantage of the deterioration by the photocorrosion[133] and might have contained harmful heavy metal elements. Therefore, when designing photocatalysts, these characteristics need to be considered.

3.3.2 Composite materials with metal oxides/organics/carbonitrides. TiO_2 is a common and stable material, which is broadly researched in the photocatalytic field, and MIL-125 could be converted into TiO_2 under specific reaction conditions like pyrolysis. Zhang *et al.*[116] prepared MIL-125-NH_2 *via* a solvothermal route and subsequently solvothermally treated it with an ethanol solution of mixed TAA. Such a post-solvothermal route made the highly active TiO_2 nanosheets coat on MIL-125-NH_2, and then a core–shell structure was formed. A large number of linker defects and many oxygen vacancies were introduced in the composite, and consequently, the photocatalytic activity was improved. The hydrogen evolution rate of the photocatalyst was 70 times that of pristine MIL-125-NH_2. In addition, the stability of the photocatalyst was improved by the core–shell structure because the more stable coated TiO_2 protected the inner core of the MOF. Sun *et al.*[134] synthesized TiO_2@MIL-125-NH_2 photocatalysts *via* a directional hydrolytic etching route, which created four exposed {100} active surfaces of MIL-125-NH_2 and resulted in enhanced photocatalytic activity. First, MIL-125-NH_2 was mixed with proper proportion of tannic acid and water, and then treated the mixed solution *via* a hydrothermal route, and finally, the sample was obtained by centrifugation and drying. Etching MIL-125-NH_2 from the inside out created an open electron transfer channel, which promoted the separation and transfer of carriers. The system provided a different route to synthesize composite materials with enhanced photocatalytic activity and high stability. Zhang *et al.*[135] found the unusual photocatalytic mechanism in MoO_3/MIL-125-NH_2 and V_2O_5/MIL-125-NH_2 composites. Different from common composite materials, both MoO_3 and V_2O_5 cannot absorb visible light or collect electrons, but the energy bands were bent in the composites, and it resulted in the formation of built-in electric field which promoted charge separation.

Covalent organic frameworks (COFs) had great potential in the field of photocatalysis.[136–138] Li *et al.*[139] fabricated a hierarchical porous metal–organic framework/covalent organic framework (MOF/COF) hybrid material *via* a post-synthetic covalent modification route (Fig. 9(a)). A benzoic acid–modified covalent triazine-based framework (B-CTF-1) was covalently bonded to MIL-125-NH_2 by amide bonds (Fig. 9(b)). It can be observed that 15T/BC had the best light absorption ability (Fig. 9(c)), which was beneficial for photocatalytic hydrogen evolution. The optimized transport pathway of photogenerated carriers resulted in the enhanced photocatalytic activity, which was over 2 times more than that of B-CTF-1 (Fig. 9(d)). The stability of the photocatalyst was significantly improved because the amide bonds were more stable than the simple heterostructure connected by van der Waals force. Compared with the rapid decaying of 15T/BC and T/C, 15TBC still maintained a high photocatalytic activity after 16 hours of reaction (Fig. 9(e)).

g-C_3N_4 was a metal-free polymer semiconductor with a medium band gap and visible light response, and hence, it was widely researched in many fields especially the field of photocatalysis. g-C_3N_4 nanosheets could compound with MIL-125-NH_2 and form the heterojunction with hierarchical porous structure.[119] The formation of the heterojunction resulted in the red-shifted light absorption region and the

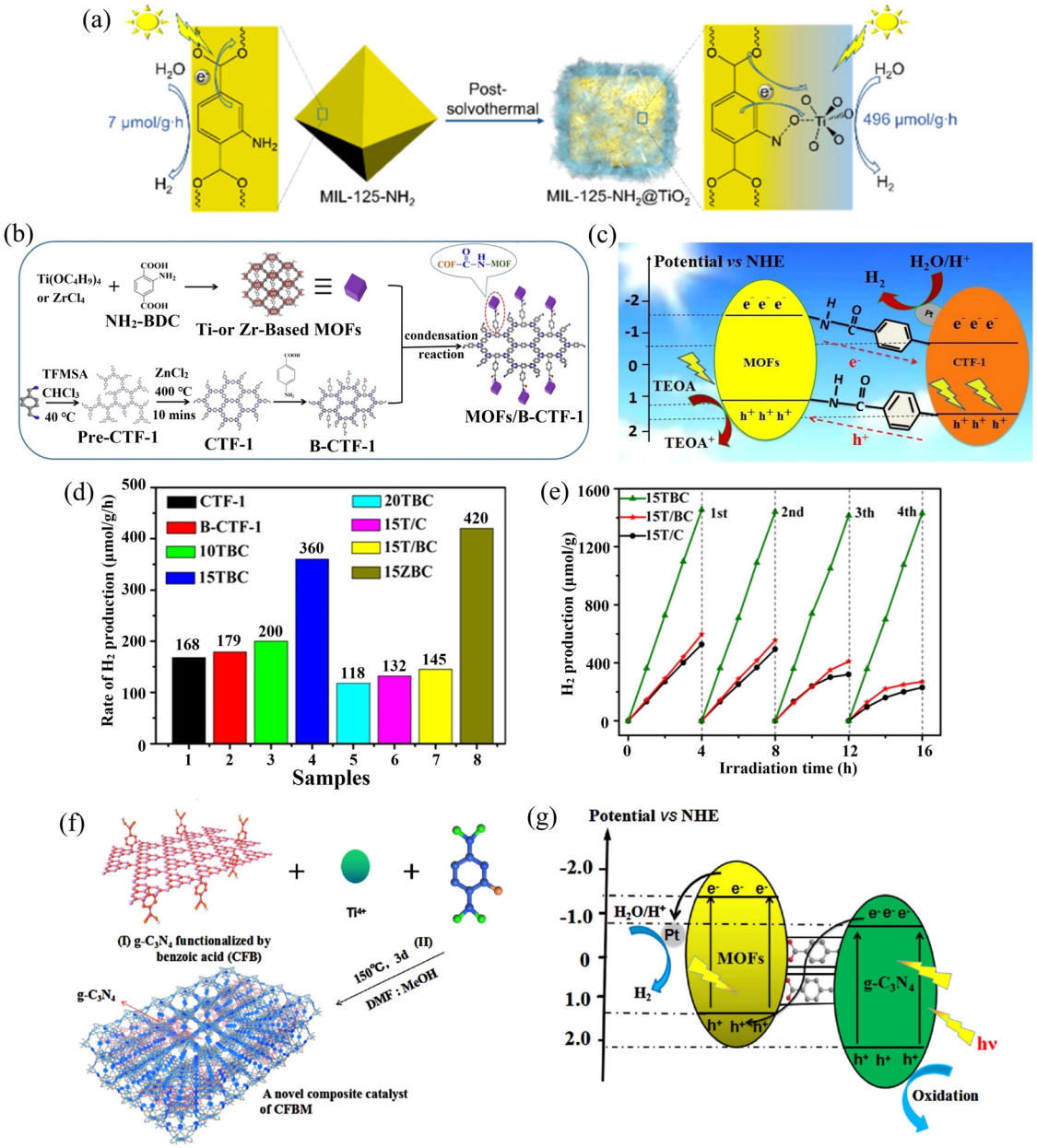

Fig. 9 (a) Schematic diagram of the synthesis process and hydrogen evolution of MIL-125-NH_2@TiO_2. Reproduced with permission from ref. 116. Copyright 2018, American Chemical Society. (b) Schematic illustration of the formation of TBC hybrid materials. (c) Photocatalytic mechanism of charge transfer for hydrogen evolution over 15TBC. (d) Rate of hydrogen evolution over different samples. (e) Cycling runs of the as-prepared catalysts. Reproduced with permission from ref. 139. Copyright 2018, Elsevier. (f) Schematic representation of the synthesis of covalently linked CFBM composites. (I) g-C_3N_4 functionalized with benzoic acid (CFB) and (II) *in situ* growth of CFBM crystals. (g) Photocatalytic mechanism of the charge transfer for hydrogen evolution over the 10CFBM under visible light irradiation. Reproduced with permission from ref. 140. Copyright 2017, Elsevier.

improved electron transfer efficiency, which enhanced the photocatalytic activity. Xu *et al.*[141] found that in the MIL-125-NH_2/g-C_3N_4/NiPd photocatalyst, the formation of close contact between MIL-125-NH_2 and g-C_3N_4 improved the electron transfer efficiency, and the loaded NiPd nanoparticles, the sensitizer, improved the light absorption and then promoted the effective separation of charges. The enhanced hydrogen evolution rate was 8.7 mmol h^{-1} g^{-1}, which was 322 times that of MIL-125-NH_2/0.75 g-C_3N_4 and 1.3 times that of MIL-125-NH_2/$Ni_{15.8}Pd_{4.1}$. However, the stability of the photocatalyst was not good. Zhou *et al.*[140] used a thermal oxidation route and an ice bath route to synthesize g-C_3N_4 functionalized by benzoic acid (CFB), and then used a two-step hydrothermal synthesis route to synthesize *Z*-scheme heterojunction photocatalysts, CFB/MIL-125-NH_2, among which CFB was linked with MIL-125-NH_2 *via* covalent bonds (Fig. 9(f)). Benzoic acid was an electron mediator that separated the carriers well and improved the electron transfer efficiency, and covalent bonds enhanced the stability of the photocatalyst (Fig. 9(g)). The hydrogen evolution rate was about 6 times that of pristine MIL-125-NH_2.

Table 4 Summary of the relevant information on MIL-125 composite photocatalysts for photocatalytic hydrogen evolution in reported publications

Photocatalysts	Specific surface area(m^2 g^{-1})	Bandgap (eV)	Irradiation	Sacrificial agents	Cocatalysts	H_2 evolution rate (mmol h^{-1} g^{-1})	Ref.
NH_2-MIL-125/Co(dmgH)$_2$	1415.28	—	Visible	TEOA	—	2.195	87
MIL-125-NH_2@TiO_2	780	—	Visible	TEOA	—	0.496	116
Cu_2O/NH_2-MIL-125	689	2.5	Solar light	TEOA	Cu_2O	11.055	117
CdS/MIL-125	349	2.8	UV-vis	lactic acid	Pt	0.25–0.30	118
NH_2-MIL-125/Pt/g-C_3N_4	64.7	—	Visible	TEOA	Pt	3.986	119
NH_2-MIL-125/ZnCr-LDH	513	2.69	Visible	TEOA	—	127.6	120
MIL-167/MIL-125-NH_2	1230	—	Visible	TEA	—	0.455	121
NH_2-MIL-125/CdS	277.54	2.50	Visible	Na_2S/Na_2SO_3	—	6.62	125
C_{60}-mediated NH_2-MIL-125/$Zn_{0.5}Cd_{0.5}S$	841.42	2.23	Visible	TEOA	—	7.825	128
NH_2-MIL-125/TiO_2/CdS	636	~2.3	Visible	Na_2S/Na_2SO_3	Pt	2.997	130
NH_2-MIL-125@$ZnIn_2S_4$/CdS	877	~1.84	Visible	MeOH	—	2.367	132
TiO_2@NH_2-MIL-125	—	—	Solar light	TEOA	—	0.440	134
NH_2-MIL-125/g-C_3N_4/NiPd	—	—	Solar light	TEOA	NiPd	8.7	141
CFB/NH_2-MIL-125	269.2	—	Visible	TEOA	Pt	1.123	140
NH_2-MIL-125/B-CTF-1	—	—	Solar light	TEOA	Pt	0.360	139
$Zn_{0.5}Cd_{0.5}S$/MIL-125-NH_2	208.7	—	Visible	Na_2S/Na_2SO_3	—	92.498	142
$ZnIn_2S_4$@NH_2-MIL-125	521.8	2.55	Visible	Na_2S/Na_2SO_3	—	2.204	143
MoO_3/MIL-125-NH_2	837	2.65	Visible	TEA	—	0.399	135

By constructing heterojunctions, the MIL-125 composite photocatalyst would have the optimized electron transfer pathway, and it can have the improved stability if the strong bonds are established. The synthesis steps of MIL-125 composite photocatalysts are relatively cumbersome, and the high stability was important in constructing composite photocatalysts.

Relevant information on the study of MIL-125 composite photocatalysts is summarized in Table 4.

4. Conclusions and prospects

This paper reviewed the research progress of MIL-125 in the field of photocatalytic hydrogen evolution. It can be concluded that MIL-125 has broad application prospects in the field of photocatalytic water splitting for hydrogen evolution. The photocatalysts based on MIL-125 had enhanced visible light response and the porous structure of MIL-125 provided a large number of active sites, which could enhance the photocatalytic activity. However, MIL-125 had its limitations. The biggest challenge was the limited photoresponse, and the rapid recombination of carriers as well as relatively poor chemical stability in aqueous solutions was also a limitation in practice. To solve these problems, various modification methods were developed including engineering functional groups and surface structure, doping metal ions, loading cocatalysts and structuring composites, and they were effective methods for improving the photocatalytic activity and the stability. It can be concluded that improving the carrier separation and transfer efficiency is central to enhancing the photocatalytic activity, and the enhanced stability depends on the optimized structure of the photocatalysts, superior bonding and other factors. These research studies are of great significance for the further development of MOF materials in photocatalysis.

In the field of photocatalytic hydrogen evolution, MIL-125 might be developed in the following five directions: (1) take effective ways to improve the stability, such as building strong bonds to replace the original weak bonds, synthesizing functional close contact structures like core–shell structures. (2) Develop derivative materials of MIL-125. Porous TiO_2 obtained by the pyrolysis of MIL-125 is a promising photocatalytic material, which has massive active sites and high stability. (3) The widespread use of noble metals increased the cost of materials and limited the large-scale application. Therefore, more research on non-noble metals and carbon materials in the field of photocatalysis is essential. (4) Carry out more experiments and theoretical calculations to research photocatalytic materials. More thorough comprehensive explorations and research studies on the internal mechanism of the photocatalytic reaction will build a more solid theoretical basis for future research. (5) In addition to high activity and high stability, the photocatalysts also need to be developed in the direction of environmental protection, low price, and large-scale production.

MIL-125 was continuously developed over the past 10 years, and it showed great potential in photocatalysis. However, its development is still in its infancy, with many unknowns to be explored and shortcomings to be overcome. It is believed that MIL-125 can be used to achieve greater success in the future.

Author contributions

Yijun He: investigation, conceptualization, writing – review & editing, writing – original draft. Tianping Lv: investigation, conceptualization, writing – review & editing, writing – original draft. Bin Xiao: writing – review & editing. Bo Liu: writing – review & editing. Tong Zhou: writing – review & editing. Jin Zhang: writing – review & editing. Yumin Zhang: writing – review & editing. Genlin Zhang: conceptualization, supervision, writing – review & editing. Qingju Liu: conceptualization, supervision, writing – review & editing.

Conflicts of interest

The author declares that they have no conflict of interest that could influence the work in this paper.

Acknowledgements

The authors thank the Advanced Analysis and Measurement Center of Yunnan University for the sample testing service. This work was funded by the Yunnan Yunling Scholars Project, the National Natural Science Foundation of China (no. 51562038), the Young and middle-aged academic and technical leaders reserve talent project in Yunnan Province (202005AC160015), the Yunnan basic applied research project (no. 202101AT070013), and the National Key Research and Development Program of China (2022YFB3803600).

References

1 C. Zheng and D. M. Kammen, *Energy Policy*, 2014, **67**, 159–169.
2 K. Berijani, A. Morsali and H. Garcia, *Microporous Mesoporous Mater.*, 2023, **349**, 112410.
3 H. C. Gulbalkan, Z. P. Haslak, C. Altintas, A. Uzun and S. Keskin, *Chem. Eng. J.*, 2022, **428**, 131239.
4 C. Pettinari, R. Pettinari, C. Di Nicola, A. Tombesi, S. Scuri and F. Marchetti, *Coord. Chem. Rev.*, 2021, **446**, 214121.
5 C. Li, W. Yang, X. Zhang, Y. Han, W. Tang, T. Yue and Z. Li, *J. Mater. Chem. C*, 2020, **8**, 2054–2064.
6 J. Zhou, C. Zeng, H. Ou, Q. Yang, Q. Xie, A. Zeb, X. Lin, Z. Ali and L. Hu, *J. Mater. Chem. C*, 2021, **9**, 11030–11058.
7 Y. Kataoka, K. Sato, Y. Miyazaki and K. Masuda, *Energy Environ. Sci.*, 2009, **2**, 397–400.
8 Z. Wang, Z. Jin, G. Wang and B. Ma, *Int. J. Hydrogen Energy*, 2018, **43**, 13039–13050.
9 T. Li, L. Zhang, X. Li, X. Wang and Z. Jin, *J. Mater. Chem. C*, 2022, **10**, 8750–8761.
10 D. Shi, R. Zheng, M. J. Sun, X. Cao, C. X. Sun, C. J. Cui, C. S. Liu, J. Zhao and M. Du, *Angew. Chem., Int. Ed.*, 2017, **56**, 14637–14641.
11 Y. Feng, C. Chen, Z. Liu, B. Fei, P. Lin, Q. Li, S. Sun and S. Du, *J. Mater. Chem. A*, 2015, **3**, 7163–7169.
12 Q. Shang, N. Liu, D. You, Q. Cheng, G. Liao and Z. Pan, *J. Mater. Chem. C*, 2021, **9**, 238–248.
13 Y. Xiao, Y. Qi, X. Wang, X. Wang, F. Zhang and C. Li, *Adv. Mater.*, 2018, **30**, 1803401.
14 H. Assi, L. C. Pardo Perez, G. Mouchaham, F. Ragon, M. Nasalevich, N. Guillou, C. Martineau, H. Chevreau, F. Kapteijn, J. Gascon, P. Fertey, E. Elkaim, C. Serre and T. Devic, *Inorg. Chem.*, 2016, **55**, 7192–7199.
15 O. Guselnikova, A. Trelin, E. Miliutina, R. Elashnikov, P. Sajdl, P. Postnikov, Z. Kolska, V. Svorcik and O. Lyutakov, *ACS Appl. Mater. Interfaces*, 2020, **12**, 28110–28119.
16 K. Mori, J. Aoyama, M. Kawashima and H. Yamashita, *Dalton Trans.*, 2014, **43**, 10541–10547.
17 Y. Guo, J. Zhang, L. Z. Dong, Y. Xu, W. Han, M. Fang, H. K. Liu, Y. Wu and Y. Q. Lan, *Chem. – Eur. J.*, 2017, **23**, 15518–15528.
18 F. Leng, H. Liu, M. Ding, Q.-P. Lin and H.-L. Jiang, *ACS Catal.*, 2018, **8**, 4583–4590.
19 L. Shen, M. Luo, L. Huang, P. Feng and L. Wu, *Inorg. Chem.*, 2015, **54**, 1191–1193.
20 L. Li, X. S. Wang, T. F. Liu and J. Ye, *Small Methods*, 2020, **4**, 2000486.
21 N. Kolobov, M. G. Goesten and J. Gascon, *Angew. Chem., Int. Ed.*, 2021, **60**, 26038–26052.
22 Y. Zhao and D. Li, *J. Mater. Chem. C*, 2020, **8**, 12739–12754.
23 M. Dan-Hardi, C. Serre, T. Frot, L. Rozes, G. Maurin, C. Sanchez and G. Férey, *J. Am. Chem. Soc.*, 2009, **131**, 10857–10859.
24 S. Smolders, T. Willhammar, A. Krajnc, K. Sentosun, M. T. Wharmby, K. A. Lomachenko, S. Bals, G. Mali, M. B. J. Roeffaers, D. E. De Vos and B. Bueken, *Angew. Chem., Int. Ed.*, 2019, **58**, 9160–9165.
25 X. Zhang, Y. Liu, Y. Pang, M. Gao and H. Pan, *J. Mater. Chem. A*, 2014, **2**, 1847–1854.
26 M. Wen, G. Li, H. Liu, J. Chen, T. An and H. Yamashita, *Environ. Sci.: Nano*, 2019, **6**, 1006–1025.
27 S.-N. Kim, J. Kim, H.-Y. Kim, H.-Y. Cho and W.-S. Ahn, *Catal. Today*, 2013, **204**, 85–93.
28 Y.-C. Zhou, P. Wang, H. Fu, C. Zhao and C.-C. Wang, *Chin. Chem. Lett.*, 2020, **31**, 2645–2650.
29 T. Xia, Y. Lin, W. Li and M. Ju, *Chin. Chem. Lett.*, 2021, **32**, 2975–2984.
30 N. Li, B. Wang, Y. Si, F. Xue, J. Zhou, Y. Lu and M. Liu, *ACS Catal.*, 2019, **9**, 5590–5602.
31 M. B. Chambers, X. Wang, L. Ellezam, O. Ersen, M. Fontecave, C. Sanchez, L. Rozes and C. Mellot-Draznieks, *J. Am. Chem. Soc.*, 2017, **139**, 8222–8228.
32 T. Zhang, Y. Jin, Y. Shi, M. Li, J. Li and C. Duan, *Coord. Chem. Rev.*, 2019, **380**, 201–229.
33 H. L. Nguyen, *New J. Chem.*, 2017, **41**, 14030–14043.
34 N. S. Abdul Mubarak, K. Y. Foo, R. Schneider, R. M. Abdelhameed and S. Sabar, *J. Environ. Chem. Eng.*, 2022, **10**, 106883.
35 Y. Shi, A.-F. Yang, C.-S. Cao and B. Zhao, *Coord. Chem. Rev.*, 2019, **390**, 50–75.
36 K. Yue, X. Zhang, S. Jiang, J. Chen, Y. Yang, F. Bi and Y. Wang, *J. Mol. Liq.*, 2021, **335**, 116108.
37 H. L. Nguyen, *New J. Chem.*, 2017, **41**, 14030–14043.
38 C. H. Hendon, D. Tiana, M. Fontecave, C. Sanchez, L. D'Arras, C. Sassoye, L. Rozes, C. Mellot-Draznieks and A. Walsh, *J. Am. Chem. Soc.*, 2013, **135**, 10942–10945.
39 F. Vermoortele, M. Maes, P. Z. Moghadam, M. J. Lennox, F. Ragon, M. Boulhout, S. Biswas, K. G. Laurier, I. Beurroies, R. Denoyel, M. Roeffaers, N. Stock, T. Duren, C. Serre and D. E. De Vos, *J. Am. Chem. Soc.*, 2011, **133**, 18526–18529.
40 Q. Li, F. Huang, D. Li, A. Yan, H. Dong, L. Ru, R. Wu and L. Yang, *Mater. Res. Bull.*, 2021, **133**, 111058.
41 L. Yang, J. Xing, D. Yuan, L. Li, Y. Xu and Z. Liu, *Chin. J. Catal.*, 2021, **42**, 2313–2321.
42 D. Ma, B. Li and Z. Shi, *Chin. Chem. Lett.*, 2018, **29**, 827–830.
43 R. Fatima, S. Park and J.-O. Kim, *J. Ind. Eng. Chem.*, 2020, **90**, 166–177.

44 Y. Fu, D. Sun, Y. Chen, R. Huang, Z. Ding, X. Fu and Z. Li, *Angew. Chem., Int. Ed.*, 2012, **124**, 3420–3423.
45 M. de Miguel, F. Ragon, T. Devic, C. Serre, P. Horcajada and H. Garcia, *ChemPhysChem*, 2012, **13**, 3651–3654.
46 Y. Zhang, C. Wen, X. Wu, P. F. Liu and H. G. Yang, *Chem. – Eur. J.*, 2022, **28**, e202200938.
47 Y. Horiuchi, T. Toyao, M. Saito, K. Mochizuki, M. Iwata, H. Higashimura, M. Anpo and M. Matsuoka, *J. Phys. Chem. C*, 2012, **116**, 20848–20853.
48 M. Sakar, C. C. Nguyen, M. H. Vu and T. O. Do, *ChemSusChem*, 2018, **11**, 809–820.
49 L. M. Liu, W. Y. Yang, Q. Li, S. A. Gao and J. K. Shang, *ACS Appl. Mater. Interfaces*, 2014, **6**, 5629–5639.
50 Y. Pan, J. Wang, S. Chen, W. Yang, C. Ding, A. Waseem and H.-L. Jiang, *Chem. Sci.*, 2022, **13**, 6696–6703.
51 F. Mohammadnezhad, S. Kampouri, S. K. Wolff, Y. Xu, M. Feyzi, J. H. Lee, X. Ji and K. C. Stylianou, *ACS Appl. Mater. Interfaces*, 2021, **13**, 5044–5051.
52 I. Ahmed, N. A. Khan, J. W. Yoon, J. S. Chang and S. H. Jhung, *ACS Appl. Mater. Interfaces*, 2017, **9**, 20938–20946.
53 H. J. An, M. Sarker, D. K. Yoo and S. H. Jhung, *Chem. Eng. J.*, 2019, **373**, 1064–1071.
54 S. Luo, C. Zhang, X. Liu, Y. Li, L. Tang, M. Fu, S. Wang, J. Wu, M. Xu, X. Wang and Y. He, *Chem. Eng. J.*, 2022, **432**, 134244.
55 G. Li, H. Kobayashi, S. Dekura, R. Ikeda, Y. Kubota, K. Kato, M. Takata, T. Yamamoto, S. Matsumura and H. Kitagawa, *J. Am. Chem. Soc.*, 2014, **136**, 10222–10225.
56 S. Ghosh, P. Roy, N. Karmodak, E. D. Jemmis and G. Mugesh, *Angew. Chem., Int. Ed.*, 2018, **57**, 4510–4515.
57 Q. Yang, Q. Xu and H. L. Jiang, *Chem. Soc. Rev.*, 2017, **46**, 4774–4808.
58 F. Guo, J. H. Guo, P. Wang, Y. S. Kang, Y. Liu, J. Zhao and W. Y. Sun, *Chem. Sci.*, 2019, **10**, 4834–4838.
59 H. G. Yang, C. H. Sun, S. Z. Qiao, J. Zou, G. Liu, S. C. Smith, H. M. Cheng and G. Q. Lu, *Nature*, 2008, **453**, 638–641.
60 W. Zhang, Y. Wang, L. Ling, X. Wang, H. Chang, R. Li, W. Duan and B. Liu, *Microporous Mesoporous Mater.*, 2020, **294**, 109943.
61 W. Wu, J. Zhang, W. Fan, Z. Li, L. Wang, X. Li, Y. Wang, R. Wang, J. Zheng, M. Wu and H. Zeng, *ACS Catal.*, 2016, **6**, 3365–3371.
62 M. Matsukawa, R. Ishikawa, T. Hisatomi, Y. Moriya, N. Shibata, J. Kubota, Y. Ikuhara and K. Domen, *Nano Lett.*, 2014, **14**, 1038–1041.
63 Y. Peng, M. Geng, J. Yu, Y. Zhang, F. Tian, Y. N. Guo, D. Zhang, X. Yang, Z. Li, Z. Li and S. Zhang, *Appl. Catal., B*, 2021, **298**, 120570.
64 Q. Zhao, J. Sun, S. Li, C. Huang, W. Yao, W. Chen, T. Zeng, Q. Wu and Q. Xu, *ACS Catal.*, 2018, **8**, 11863–11874.
65 H. Wu, Y. S. Chua, V. Krungleviciute, M. Tyagi, P. Chen, T. Yildirim and W. Zhou, *J. Am. Chem. Soc.*, 2013, **135**, 10525–10532.
66 J. Choi, L.-C. Lin and J. C. Grossman, *J. Phys. Chem. C*, 2018, **122**, 5545–5552.
67 X. Zheng, G. Jia, G. Fan, W. Luo, Z. Li and Z. Zou, *Small*, 2020, **16**, 2003630.
68 J. Xu, L. Lu, C. Zhu, Q. Fang, R. Liu, D. Wang, Z. He, S. Song and Y. Shen, *J. Colloid Interface Sci.*, 2023, **630**, 430–442.
69 Y. Zhao, Q. Zhang, Y. Li, R. Zhang and G. Lu, *ACS Appl. Mater. Interfaces*, 2017, **9**, 15079–15085.
70 M. Vandichel, J. Hajek, F. Vermoortele, M. Waroquier, D. E. De Vos and V. Van Speybroeck, *CrystEngComm*, 2015, **17**, 395–406.
71 Y. Horiuchi, K. Tatewaki, S. Mine, T.-H. Kim, S. W. Lee and M. Matsuoka, *J. Catal.*, 2020, **392**, 119–125.
72 Y. He, Y. Tan, M. Song, Q. Tu, M. Fu, L. Long, J. Wu, M. Xu and X. Liu, *J. Hazard. Mater.*, 2022, **430**, 128468.
73 S. Naghdi, A. Cherevan, A. Giesriegl, R. Guillet-Nicolas, S. Biswas, T. Gupta, J. Wang, T. Haunold, B. C. Bayer, G. Rupprechter, M. C. Toroker, F. Kleitz and D. Eder, *Nat. Commun.*, 2022, **13**, 282.
74 Z. Gao, J. Wang, Y. Muhammad, Y. Zhang, S. J. Shah, Y. Hu, Z. Chu, Z. Zhao and Z. Zhao, *Chem. Eng. J.*, 2020, **388**, 124389.
75 Z. Wei, B. Ding, H. Dou, J. Gascon, X.-J. Kong, Y. Xiong, B. Cai, R. Zhang, Y. Zhou, M. Long, J. Miao, Y. Dou, D. Yuan and J. Ma, *Chin. Chem. Lett.*, 2019, **30**, 2110–2122.
76 L. Xia, W. Zhou, Y. Xu, Z. Xia, X. Wang, Q. Yang, G. Xie, S. Chen and S. Gao, *Chem. Eng. J.*, 2023, **451**, 138747.
77 X. Chen, S. Xiao, H. Wang, W. Wang, Y. Cai, G. Li, M. Qiao, J. Zhu, H. Li, D. Zhang and Y. Lu, *Angew. Chem., Int. Ed.*, 2020, **59**, 17182–17186.
78 H. Li, X. Liu, H. Feng, J. Zhao, P. Lu, M. Fu, W. Guo, Y. Zhao and Y. He, *Catal. Sci. Technol.*, 2021, **11**, 6225–6233.
79 Y. Zhang, F. Mao, Y. Liu, X. Wu, C. Wen, S. Dai, P. Liu and H. Yang, *Sci. China Mater.*, 2021, **65**, 1237–1244.
80 P. Karthik, A. R. M. Shaheer, A. Vinu and B. Neppolian, *Small*, 2020, **16**, 1902990.
81 W. Zhou, W. Li, J. Q. Wang, Y. Qu, Y. Yang, Y. Xie, K. Zhang, L. Wang, H. Fu and D. Zhao, *J. Am. Chem. Soc.*, 2014, **136**, 9280–9283.
82 C. Tai, H. Liu and Y. Hu, *ACS Sustainable Chem. Eng.*, 2020, **8**, 18196–18205.
83 M. Martis, K. Mori, K. Fujiwara, W.-S. Ahn and H. Yamashita, *J. Phys. Chem. C*, 2013, **117**, 22805–22810.
84 S. Kampouri, T. N. Nguyen, M. Spodaryk, R. G. Palgrave, A. Züttel, B. Smit and K. C. Stylianou, *Adv. Funct. Mater.*, 2018, **28**, 1806368.
85 S. Falletta, P. Gono, Z. Guo, S. Kampouri, K. C. Stylianou and A. Pasquarello, *J. Mater. Chem. A*, 2020, **8**, 20493–20502.
86 R. A. Marcus, *Rev. Mod. Phys.*, 1993, **65**, 599–610.
87 S. Luo, X. Liu, X. Wei, M. Fu, P. Lu, X. Li, Y. Jia, Q. Ren and Y. He, *J. Hazard. Mater.*, 2020, **399**, 122824.
88 Y. He, S. Luo, Y. Tan, M. Chen, H. Zhou, J. Yu, L. Pu, Y. Huang, M. Fu and X. Liu, *J. Alloys Compd.*, 2022, **913**, 165226.
89 A. Fihri, V. Artero, M. Razavet, C. Baffert, W. Leibl and M. Fontecave, *Angew. Chem., Int. Ed.*, 2008, **47**, 564–567.
90 S. Sk, I. Mondal, A. Mahata, B. M. Abraham, C. Nayak, D. Bhattacharyya, S. N. Jha, R. Ghosh and U. Pal, *ACS Appl. Energy Mater.*, 2022, **5**, 12324–12335.

91 P. Roy, P.-C. Chen, A. P. Periasamy, Y.-N. Chen and H.-T. Chang, *Mater. Today*, 2015, **18**, 447–458.
92 M. Tuerhong, Y. Xu and X.-B. Yin, *Chin. J. Anal. Chem.*, 2017, **45**, 139–150.
93 S. Liu, J. Tian, L. Wang, Y. Zhang, X. Qin, Y. Luo, A. M. Asiri, A. O. Al-Youbi and X. Sun, *Adv. Mater.*, 2012, **24**, 2037–2041.
94 L. Bao, Z. L. Zhang, Z. Q. Tian, L. Zhang, C. Liu, Y. Lin, B. Qi and D. W. Pang, *Adv. Mater.*, 2011, **23**, 5801–5806.
95 Y. Zhang, J. Zhao, H. Wang, B. Xiao, W. Zhang, X. Zhao, T. Lv, M. Thangamuthu, J. Zhang, Y. Guo, J. Ma, L. Lin, J. Tang, R. Huang and Q. Liu, *Nat. Commun.*, 2022, **13**, 58.
96 J. D. Xiao, L. Han, J. Luo, S. H. Yu and H. L. Jiang, *Angew. Chem., Int. Ed.*, 2018, **57**, 1103–1107.
97 Y. An, B. Xu, Y. Liu, Z. Wang, P. Wang, Y. Dai, X. Qin, X. Zhang and B. Huang, *ChemistryOpen*, 2017, **6**, 701–705.
98 X. Huang, X. Li, Q. Luan, K. Zhang, Z. Wu, B. Li, Z. Xi, W. Dong and G. Wang, *Nano Res.*, 2021, **14**, 4250–4257.
99 J. Qiu, L. Yang, M. Li and J. Yao, *Mater. Res. Bull.*, 2019, **112**, 297–306.
100 M. A. Nasalevich, R. Becker, E. V. Ramos-Fernandez, S. Castellanos, S. L. Veber, M. V. Fedin, F. Kapteijn, J. N. H. Reek, J. I. van der Vlugt and J. Gascon, *Energy Environ. Sci.*, 2015, **8**, 364–375.
101 A. Iglesias-Juez, S. Castellanos, M. Monte, G. Agostini, D. Osadchii, M. A. Nasalevich, J. G. Santaclara, A. I. Olivos Suarez, S. L. Veber, M. V. Fedin and J. Gascón, *J. Mater. Chem. A*, 2018, **6**, 17318–17322.
102 Z. Li, J.-D. Xiao and H.-L. Jiang, *ACS Catal.*, 2016, **6**, 5359–5365.
103 Y. He, S. Luo, X. Hu, Y. Cheng, Y. Huang, S. Chen, M. Fu, Y. Jia and X. Liu, *Chem. Eng. J.*, 2021, **420**, 127643.
104 Y. Chen, S. Ji, C. Chen, Q. Peng, D. Wang and Y. Li, *Joule*, 2018, **2**, 1242–1264.
105 Y. Ma, Y. Zhang, Y. Ma, T. Lv, B. Xiao, X. Kuang, X. Deng, J. Zhang, J. Zhao and Q. Liu, *Nanoscale*, 2022, **14**, 15889–15896.
106 Y. Ma, Y. Ma, T. Lv, X. Deng, X. Kuang, J. Zhang, Q. Liu and Y. Zhang, *Catal. Sci. Technol.*, 2022, **12**, 3856–3862.
107 T. Wang, X. Tao, X. Li, K. Zhang, S. Liu and B. Li, *Small*, 2021, **17**, 2006255.
108 T. Lv, B. Xiao, F. Xia, M. Chen, J. Zhao, Y. Ma, J. Wu, J. Zhang, Y. Zhang and Q. Liu, *Chem. Eng. J.*, 2022, **450**, 137873.
109 B. Yan, D. Liu, X. Feng, M. Shao and Y. Zhang, *Adv. Funct. Mater.*, 2020, **30**, 2003007.
110 S. Kampouri, T. N. Nguyen, C. P. Ireland, B. Valizadeh, F. M. Ebrahim, G. Capano, D. Ongari, A. Mace, N. Guijarro, K. Sivula, A. Sienkiewicz, L. Forró, B. Smit and K. C. Stylianou, *J. Mater. Chem. A*, 2018, **6**, 2476–2481.
111 T. N. Nguyen, S. Kampouri, B. Valizadeh, W. Luo, D. Ongari, O. M. Planes, A. Zuttel, B. Smit and K. C. Stylianou, *ACS Appl. Mater. Interfaces*, 2018, **10**, 30035–30039.
112 Y. Li, Z. Jin, X. Hao and G. Wang, *Int. J. Hydrogen Energy*, 2019, **44**, 17909–17921.
113 S. Remiro-Buenamañana, M. Cabrero-Antonino, M. Martínez-Guanter, M. Álvaro, S. Navalón and H. García, *Appl. Catal., B*, 2019, **254**, 677–684.
114 D. Chi, Y. Ma, H. Fang, R. Chen, Y. Chen, B. Liu, S. Liu and K. Zhang, *Int. J. Hydrogen Energy*, 2023, **48**, 2583–2592.
115 Y. He, H. Li, J. Wu, Z. Liu, Y. Chen, W. Guo, Y. Wu, M. Fu and X. Liu, *Appl. Surf. Sci.*, 2022, **604**, 154641.
116 B. Zhang, J. Zhang, X. Tan, D. Shao, J. Shi, L. Zheng, J. Zhang, G. Yang and B. Han, *ACS Appl. Mater. Interfaces*, 2018, **10**, 16418–16423.
117 P. Karthik, E. Balaraman and B. Neppolian, *Catal. Sci. Technol.*, 2018, **8**, 3286–3294.
118 A. Rahmani, H. B. M. Emrooz, S. Abedi and A. Morsali, *Mater. Sci. Semicond. Process.*, 2018, **80**, 44–51.
119 Z. Su, B. Zhang, J. Shi, D. Tan, F. Zhang, L. Liu, X. Tan, D. Shao, G. Yang and J. Zhang, *Sustainable Energy Fuels*, 2019, **3**, 1233–1238.
120 M. Sohail, H. Kim and T. W. Kim, *Sci. Rep.*, 2019, **9**, 7584.
121 S. Kampouri, F. M. Ebrahim, M. Fumanal, M. Nord, P. A. Schouwink, R. Elzein, R. Addou, G. S. Herman, B. Smit, C. P. Ireland and K. C. Stylianou, *ACS Appl. Mater. Interfaces*, 2021, **13**, 14239–14247.
122 R. Marschall, *Adv. Funct. Mater.*, 2014, **24**, 2421–2440.
123 J. Chen, X. J. Wu, L. Yin, B. Li, X. Hong, Z. Fan, B. Chen, C. Xue and H. Zhang, *Angew. Chem., Int. Ed.*, 2015, **54**, 1210–1214.
124 C. Dispenza, N. Grimaldi, M. A. Sabatino, I. L. Soroka and M. Jonsson, *J. Nanosci. Nanotechnol.*, 2015, **15**, 3445–3467.
125 X. Zhang, Z. Chen, Y. Luo, X. Han, Q. Jiang, T. Zhou, H. Yang and J. Hu, *J. Hazard. Mater.*, 2021, **405**, 124128.
126 W. Jiang, X. Zong, L. An, S. Hua, X. Miao, S. Luan, Y. Wen, F. F. Tao and Z. Sun, *ACS Catal.*, 2018, **8**, 2209–2217.
127 S. Liu, X. Jiang, G. I. N. Waterhouse, Z.-M. Zhang and L.-M. Yu, *Sep. Purif. Technol.*, 2022, **294**, 121094.
128 C. Li, X. Liu, P. Huo, Y. Yan, G. Liao, G. Ding and C. Liu, *Small*, 2021, **17**, 2102539.
129 L. Song, T. Li and S. Zhang, *J. Phys. Chem. C*, 2016, **121**, 293–299.
130 R. Bibi, H. Huang, M. Kalulu, Q. Shen, L. Wei, O. Oderinde, N. Li and J. Zhou, *ACS Sustainable Chem. Eng.*, 2018, **7**, 4868–4877.
131 B. Sun, W. Zhou, H. Li, L. Ren, P. Qiao, W. Li and H. Fu, *Adv. Mater.*, 2018, **30**, 1804282.
132 S. Zhang, M. Du, Z. Xing, Z. Li, K. Pan and W. Zhou, *Appl. Catal., B*, 2020, **262**, 118202.
133 C. Cui, G. Li and Z. Tang, *Chin. Chem. Lett.*, 2021, **32**, 3307–3321.
134 L. Sun, Y. Yuan, F. Wang, Y. Zhao, W. Zhan and X. Han, *Nano Energy*, 2020, **74**, 104909.
135 C. Zhang, C. Xie, Y. Gao, X. Tao, C. Ding, F. Fan and H. L. Jiang, *Angew. Chem., Int. Ed.*, 2022, **61**, e202204108.
136 U. Díaz and A. Corma, *Coord. Chem. Rev.*, 2016, **311**, 85–124.
137 R. K. Sharma, P. Yadav, M. Yadav, R. Gupta, P. Rana, A. Srivastava, R. Zbořil, R. S. Varma, M. Antonietti and M. B. Gawande, *Mater. Horiz.*, 2020, **7**, 411–454.

138 M.-X. Wu and Y.-W. Yang, *Chin. Chem. Lett.*, 2017, **28**, 1135–1143.
139 F. Li, D. Wang, Q. Xing, G. Zhou, S. Liu, Y. Li, L. Zheng, P. Ye and J. Zou, *Appl. Catal., B*, 2019, **243**, 621–628.
140 G. Zhou, M. Wu, Q. Xing, F. Li, H. Liu, X. Luo, J. Zou, J. Luo and A. Zhang, *Appl. Catal., B*, 2018, **220**, 607–614.
141 J. Xu, J. Gao, C. Wang, Y. Yang and L. Wang, *Appl. Catal., B*, 2017, **219**, 101–108.
142 Y. Guo, J. Li, X. Yang, Y. Lou and J. Chen, *Inorg. Chem. Commun.*, 2020, **112**, 107714.
143 H. Liu, J. Zhang and D. Ao, *Appl. Catal., B*, 2018, **221**, 433–442.